Fermionic next-to-next-to leading logarithmic corrections to $b\to s\gamma$

Kay Bieri* and Christoph Greub†
Institut für Theoretische Physik, Universität Bern, CH-3012 Bern, Switzerland

Matthias Steinhauser
II. Institut für Theoretische Physik, Universität Hamburg, D-22761 Hamburg, Germany

(Received 7 February 2003; published 20 June 2003)

In this paper we take the first step towards a complete next-to-next-to-leading logarithmic (NNLL) calculation of the inclusive decay rate for $B\to X_s\gamma$. We consider the virtual corrections of the order of $\alpha_s^2 n_f$ to the matrix elements of the operators O_1, O_2 and O_8 and evaluate the real and virtual contributions to O_7. These corrections are expected to be numerically important. We observe a strong cancellation between the contributions from the current-current operators and O_7 and obtain, after applying naive non-Abelianization, a reduction of the branching ratio of 3.9% (for $\mu=3.0$ GeV) and an increase of 3.4% (for $\mu=9.6$ GeV).

DOI: 10.1103/PhysRevD.67.114019 PACS number(s): 13.25.Hw, 12.38.Bx, 14.65.Fy

I. INTRODUCTION

Currently, measurements of the inclusive branching ratio BR($B\to X_s\gamma$) are provided by CLEO [1] (Cornell), by the B factory Belle [2] (KEK), by ALEPH [3] (CERN), and by the preliminary BABAR [4,5] (SLAC) results, leading to a world average of [6]

$$\mathrm{BR}(B\to X_s\gamma)_{\mathrm{exp}}=(3.34\pm 0.38)\times 10^{-4}. \tag{1}$$

This experimental average is in good agreement with the theoretical prediction based on the standard model (SM) including next-to-leading logarithmic (NLL) QCD corrections supplemented by certain classes of leading order electroweak terms [7–10]. For a recent status report on inclusive rare B decays and a complete list of references on NLL calculations of BR(B$\to$ $X_s\gamma$) the reader is referred to Ref. [11]. In earlier analyses [8,12–15], the ratio m_c/m_b, which enters the calculation of the decay width $\Gamma(B\to X_s\gamma)$ for the first time at the NLL level, was tacitly interpreted to be the ratio of the pole quark masses. Using $m_c/m_b=0.29\pm 0.02$, one obtains $\mathrm{BR}(B\to X_s\gamma)_{\mathrm{SM}}=(3.35\pm 0.30)\times 10^{-4}$, where the errors due to the uncertainties in the various input parameters and the estimated uncertainties due to the left-over renormalization scale dependence were added in quadrature. More recently, Gambino and Misiak [16] pointed out that the branching ratio rises to $\mathrm{BR}(B\to X_s\gamma)_{\mathrm{SM}}=(3.73\pm 0.30)\times 10^{-4}$ [16] (see also Ref. [17]), if one interprets m_c/m_b to be $\overline{m}_c(\mu)/m_b=0.22\pm 0.04$, where $\overline{m}_c(\mu)$ is the charm quark mass in the modified minimal subtraction ($\overline{\mathrm{MS}}$) scheme, evaluated at a scale μ in the range $m_c<\mu<m_b$, and m_b is the bottom quark $1S$ mass.

Despite the current theoretical dispersion on the branching ratio, the agreement between the present experimental results and the SM is quite impressive and this has been used to derive model independent bounds on the Wilson coefficients $C_7(m_W)$ and $C_8(m_W)$ (see, for example, Ref. [18]).

Formally, the approximately 11% discrepancy in the branching ratio, stemming from the two different schemes for m_c/m_b, is a NNLL effect. As the measurements of BR($B\to X_s\gamma$) will become much more precise in the near future, it will become mandatory to systematically extend the theoretical predictions to NNLL precision, in order to fully exploit this process in the search for new physics.

To illustrate the complexity of such a calculation, we briefly explain the theoretical framework. Usually, one works in the effective field theory formalism of the SM, where the W boson and heavier degrees of freedom are integrated out. This results in an effective Hamiltonian in which operators up to dimension six are retained. Adopting the operator definition of Ref. [12], the relevant Hamiltonian to describe the processes $b\to s\gamma$, $b\to sg$, and $b\to s\gamma g$ reads

$$H_{\mathrm{eff}}=-\frac{4G_F}{\sqrt{2}}\lambda_t\sum_{i=1}^{8}C_i(\mu)O_i(\mu), \tag{2}$$

where G_F is the Fermi coupling constant, $\lambda_t=V_{ts}^{\star}V_{tb}$ (with V_{ij} being elements of the Cabibbo-Kobayashi-Maskawa matrix), and $C_i(\mu)$ are the Wilson coefficient functions evaluated at the scale μ. For practical reasons it is more convenient to use instead of the original functions $C_i(\mu)$ certain linear combinations, the so-called ''effective Wilson coefficients'' $C_i^{\mathrm{eff}}(\mu)$ introduced in Refs. [12,19]:

$$\begin{aligned}
C_i^{\mathrm{eff}}(\mu)&=C_i(\mu)\quad (i=1,\ldots,6),\\
C_7^{\mathrm{eff}}(\mu)&=C_7(\mu)+\sum_{i=1}^{6}y_iC_i(\mu),\\
C_8^{\mathrm{eff}}(\mu)&=C_8(\mu)+\sum_{i=1}^{6}z_iC_i(\mu),
\end{aligned} \tag{3}$$

where y_i and z_i are defined in such a way that the leading order matrix elements $\langle s\gamma|O_i|b\rangle$ and $\langle sg|O_i|b\rangle$ ($i=1,\ldots,6$) are absorbed in the leading order terms of $C_7^{\mathrm{eff}}(\mu)$ and $C_8^{\mathrm{eff}}(\mu)$. The explicit values of $\{y_i\}$ and $\{z_i\}$, $y=(0,0,-\frac{1}{3},-\frac{4}{9},-\frac{20}{3},-\frac{80}{9})$, $z=(0,0,1,-\frac{1}{6},20,-\frac{10}{3})$ were

*Electronic address: bierik@itp.unibe.ch
†Electronic address: greub@itp.unibe.ch

obtained in Ref. [12] in the $\overline{\rm MS}$ scheme using fully anticommuting γ_5 which is also adopted in the present paper.

The operators relevant for our calculation read

$$O_1=(\bar{s}_L\gamma_\mu T^a c_L)(\bar{c}_L\gamma^\mu T^a b_L),$$

$$O_2=(\bar{s}_L\gamma_\mu c_L)(\bar{c}_L\gamma^\mu b_L),$$

$$O_4=(\bar{s}_L\gamma_\mu T^a b_L)\sum_q (\bar{q}\gamma^\mu T^a q),$$

$$O_7=\frac{e}{16\pi^2}\bar{m}_b(\mu)(\bar{s}_L\sigma^{\mu\nu}b_R)F_{\mu\nu},$$

$$O_8=\frac{g_s}{16\pi^2}\bar{m}_b(\mu)(\bar{s}_L\sigma^{\mu\nu}T^a b_R)G^a_{\mu\nu}. \tag{4}$$

Here $e=\sqrt{4\pi\alpha_{\rm em}}$ and $g_s=\sqrt{4\pi\alpha_s}$ denote the electromagnetic and strong coupling constants, respectively. Furthermore, $F_{\mu\nu}$ and $G^a_{\mu\nu}$ are the corresponding field strength tensors and $L=(1-\gamma_5)/2$ and $R=(1+\gamma_5)/2$ stand for left- and right-handed projection operators. The factor $\bar{m}_b(\mu)$ in the definition of O_7 and O_8 denotes the bottom mass in the $\overline{\rm MS}$ scheme.

For a complete NNLL calculation in this framework, the evaluation of three parts is necessary. (1) The computation of the matching coefficients to order α_s^2 which requires a three-loop calculation. (2) The evaluation of the anomalous dimension matrix to order α_s^3 where four-loop diagrams are involved. (3) The calculation of the order α_s^2 QCD corrections to the matrix elements $\langle s\gamma|O_i(\mu)|b\rangle$ (μ is of order m_b) which, depending on the operator, is either a two- or three-loop calculation.

The relatively large dependence of the NLL prediction for ${\rm BR}(B\to X_s\gamma)_{\rm SM}$ on the scheme for m_c/m_b illustrates that NNLL effects, in particular those related to step (3), can be rather large. At this point we should stress that the issue related to the definition of m_c/m_b serves us as a motivation to initiate a NNLL calculation for ${\rm BR}(B\to X_s\gamma)$. In the present paper we are working out a class of NNLL corrections (to be specified below) to step (3), which is not related to the m_c/m_b issue. However, in many other processes it is known that the kind of terms considered in this paper are the source of very important higher order corrections.

In this paper we consider those corrections of order α_s^2 to the matrix elements for $B\to X_s\gamma$ associated with the operators O_1, O_2, O_7, and O_8 which involve a closed fermion loop. It is needless to say, that at the same time also the matching coefficients and the anomalous dimension matrix should be improved accordingly. Motivated by the fact that the NLL corrections to the matrix elements were numerically more important than the improvements in the Wilson coefficients, we assume for the time being that this could also be the case at the NNLL level. Therefore, we only concentrate on NNLL corrections to the matrix elements. In principle also the contributions from the operators O_i ($i=3,\ldots,6$) should be considered. However, as the corresponding Wilson coefficients are small, we neglect these contributions. Furthermore, we also neglect the NNLL bremsstrahlung corrections to the interferences (O_1,O_1), (O_1,O_2), (O_2,O_2), (O_1,O_7), (O_1,O_8), (O_2,O_7), (O_2,O_8), (O_7,O_8), and (O_8,O_8), since these terms are infrared finite for vanishing gluon energy and numerically relatively small at the NLL level [20].

The fermionic corrections we are interested in are essentially generated by inserting a one-loop fermion bubble into the gluon propagator of the lower order Feynman diagrams. For the numerical evaluation we will assume that $n_f=5$ massless fermions are present in the fermion loop.

Once the corrections of $\mathcal{O}(\alpha_s^2 n_f)$ are available, it is suggestive to use the hypothesis of naive non-Abelianization (NNA) [21] in order to estimate the complete corrections of order α_s^2. This is based on the observation that the lowest coefficient of the QCD β function $\beta_0=11-2n_f/3$ is quite large and thus it is expected that the replacement of n_f by $-3\beta_0/2$ may lead to a good approximation of the full order α_s^2 corrections. There are many physical observables, where NNA provides an excellent approximation to the full two-loop corrections [22,23] such as the inclusive cross section $e^+e^-\to$hadrons, the hadronic τ decay, or the two-loop relation between the $\overline{\rm MS}$ and pole quark mass. In particular, we want to mention the semileptonic decay $\Gamma(b\to c l \nu_l)$ where the deviation of the $\alpha_s^2\beta_0$ terms from the complete α_s^2 result [24] is less than 20%. We also note that the $O(\alpha_s^2\beta_0)$ corrections to the photon energy spectrum in $B\to X_s\gamma$ (away from the endpoint) were calculated in Ref. [25].

Our presentation is organized as follows. In Sec. II we discuss the virtual corrections associated with $O_{1,2}$ and compute in Sec. III both the real and virtual corrections to O_7. The virtual corrections to O_8 are considered in Sec. IV. In Sec. V we combine our findings with the existing NLL results and perform a numerical analysis showing the importance of our new terms. Finally, Sec. VI contains our conclusions. In the appendixes supplementary material is provided. Appendix A contains the building blocks which are useful for the practical calculations and in Appendix B detailed analytical results are presented for the corrections to the matrix element $\langle s\gamma|O_2|b\rangle$. For completeness the results of the order α_s corrections are listed in Appendix C and intermediate results needed for the matrix element $\langle s\gamma|O_7|b\rangle$ are given in Appendix D. In Appendix E the results are provided which are necessary to discuss the branching ratio ${\rm BR}(b\to X_s\gamma)_{E_\gamma\geq E_{\rm cut}}$ where $E_{\rm cut}$ represents a cutoff on the photon energy.

II. VIRTUAL CORRECTIONS TO $b\to s\gamma$ ASSOCIATED WITH O_1 AND O_2

In this section we derive the (renormalized) order α_s^2 corrections to the matrix elements $\langle s\gamma|O_1|b\rangle$ and $\langle s\gamma|O_2|b\rangle$. Thereby only the contributions proportional to the number of fermion flavors n_f are taken into account. We show at the

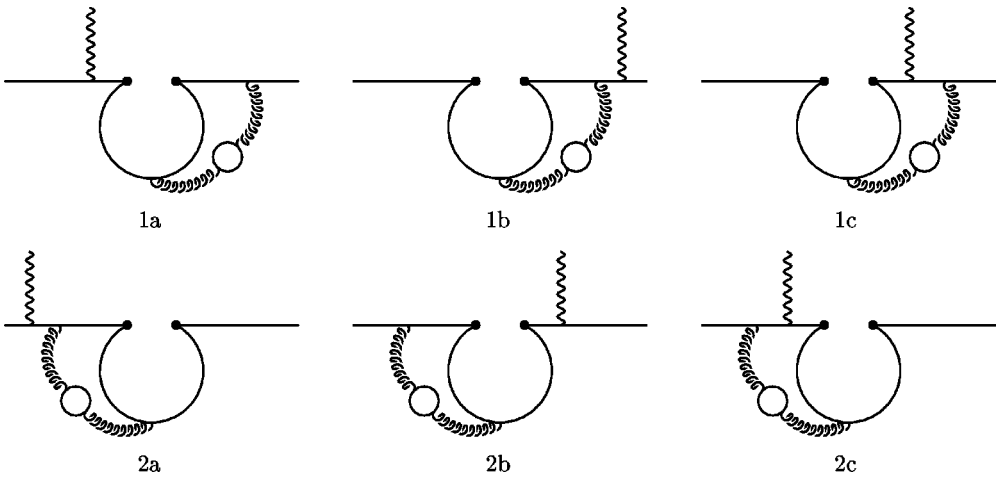

FIG. 1. Diagrams (1a)–(1c) and (2a)–(2c) associated with the operator O_2. The photon is represented by a wavy line and is emitted from a down-type quark in all the diagrams. The virtual gluons are represented by curly lines. The sum of the first three graphs is denoted with $M^{(2)}_{2,\mathrm{bare}}(1)$, whereas the sum of the second three diagrams is called $M^{(2)}_{2,\mathrm{bare}}(2)$.

end of this section that the result for $\langle s\gamma|O_1|b\rangle$ can easily be obtained from the one for $\langle s\gamma|O_2|b\rangle$. Therefore, we concentrate in the following on the calculation of the renormalized matrix element M_2

$$M_2=\langle s\gamma|O_2|b\rangle, \tag{5}$$

which is conveniently written in the form

$$M_2=M_2^{(0)}+M_2^{(1)}+M_2^{(2)}. \tag{6}$$

The superscript counts the factors of α_s. The leading term vanishes, i.e., $M_2^{(0)}=0$ and the $\mathcal{O}(\alpha_s)$ calculation has been performed in Ref. [20]. In the following, we discuss the $\mathcal{O}(\alpha_s^2 n_f)$ term $M_2^{(2)}$. In Sec. II A we present the calculation and results of the dimensionally regularized three-loop diagrams, while Sec. II B is devoted to the calculation of the counterterms. In Sec. II C we combine the results of the three-loop results with the counterterms and derive the renormalized expression $M_2^{(2)}$.

A. Regularized three-loop corrections to $\langle s\gamma|O_2|b\rangle$

The three-loop diagrams contributing to $M_2^{(2)}$ can be divided into four nonvanishing classes as shown in Figs. 1 and 2.[1] The sum of the diagrams in each class is gauge invariant. The contributions to the matrix element $M_2^{(2)}$ of the individual classes are denoted by $M^{(2)}_{2,\mathrm{bare}}(1)$, $M^{(2)}_{2,\mathrm{bare}}(2)$, $M^{(2)}_{2,\mathrm{bare}}(3)$ and $M^{(2)}_{2,\mathrm{bare}}(4)$, where, e.g., $M^{(2)}_{2,\mathrm{bare}}(1)$ is

$$M^{(2)}_{2,\mathrm{bare}}(1)=M^{(2)}_{2,\mathrm{bare}}(1a)+M^{(2)}_{2,\mathrm{bare}}(1b)+M^{(2)}_{2,\mathrm{bare}}(1c). \tag{7}$$

For the practical calculation we essentially follow the techniques developed in Ref. [20]. To make the paper self-contained, we nevertheless present as an example the calculation of the diagram (2c) in some detail.

The amplitude $M^{(2)}_{2,\mathrm{bare}}(2c)$ is constructed with the help of the building blocks I_β and $K^f_{\beta\beta'}$, shown in Fig. 9 in Appendix A. The analytic expression for I_β is given in Eq. (A1), while $K^f_{\beta\beta'}$ is given in Eq. (A2) for an arbitrary mass m_f of the quark in the loop. This mass is retained in $K^f_{\beta\beta'}$, because it will be used as a regulator of infrared singularities in the calculation of $\langle s\gamma|O_7|b\rangle$. As $\langle s\gamma|O_2|b\rangle$ is free of infrared singularities, we can put in this section $m_f=0$. Thus the parameter integral in Eq. (A2) can be expressed in terms of Euler Γ functions. Furthermore, only the $g_{\beta\beta'}$ term has to be kept as the other building block I_β is transversal. The diagram (2c) can be written as

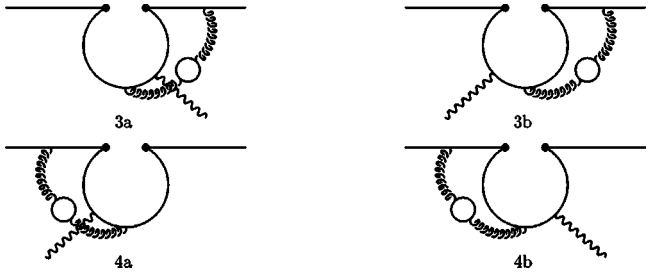

FIG. 2. Diagrams (3a)–(3b) and (4a)–(4b) associated with the operator O_2. The photon is represented by a wavy line and is emitted from an up-type quark in all the diagrams. The virtual gluons are represented by curly lines. The sum of the first two graphs is denoted with $M^{(2)}_{2,\mathrm{bare}}(3)$, whereas the sum of the second two diagrams is called $M^{(2)}_{2,\mathrm{bare}}(4)$.

[1]In principle there are also diagrams in which the photon is emitted from the quark-loop insertion in the gluon propagator. However, these contributions vanish due to Furry's theorem.

$$M_{2,\mathrm{bare}}^{(2)}(2c) = -\frac{2i}{(4\pi)^{\epsilon}}\left(\frac{\alpha_s}{\pi}\right)^2 eQ_d C_F T n_f \times \frac{\Gamma^2(\epsilon)\Gamma^2(2-\epsilon)(1-\epsilon)}{\Gamma(4-2\epsilon)} e^{2i\pi\epsilon+3\gamma_E\epsilon}\mu^{6\epsilon} \times \int \frac{d^d r}{(2\pi)^d}\overline{u}(p')(r_\beta \not{r} - r^2\gamma_\beta) \times L\frac{\not{p}'+\not{r}+m_b}{(p'+r)^2-m_b^2+i\delta}\not{\varepsilon}\frac{\not{p}+\not{r}+m_b}{(p+r)^2-m_b^2+i\delta} \times \gamma^\beta u(p)\frac{1}{(r^2+i\delta)^{1+\epsilon}}\int_0^1 dx x^{1-\epsilon}(1-x)^{1-\epsilon} \times\left(r^2-\frac{m_c^2}{x(1-x)}+i\delta\right)^{-\epsilon}, \tag{8}$$

where $u(p)$ and $u(p')$ are the Dirac spinors of the b and s quark, respectively, while ε denotes the polarization vector of the photon. C_F and T are the eigenvalue of the quadratic Casimir operator and the index of the fundamental representation of the color gauge group, respectively, with the numerical values $C_F=4/3$ and $T=1/2$. The Euler constant γ_E appears in Eq. (8), because we write the square of the renormalization scale in the form $\mu^2\exp(\gamma_E)/(4\pi)$. The parameter δ (with $\delta>0$) in the denominators of the various propagators symbolizes the "ϵ prescription."

In a next step we denote the four different denominators with

$$D_1=(p'+r)^2-m_b^2+i\delta,$$
$$D_2=(p+r)^2-m_b^2+i\delta,$$
$$D_3=r^2-\frac{m_c^2}{x(1-x)}+i\delta,$$
$$D_4=r^2+i\delta,$$

and introduce a Feynman parametrization as follows:

$$\frac{1}{D_1 D_2 D_3^{\epsilon} D_4^{1+\epsilon}} = \frac{\Gamma(3+2\epsilon)}{\Gamma(\epsilon)\Gamma(1+\epsilon)} \times \int \frac{du\,dv\,dy\,w^{\epsilon} y^{\epsilon-1}}{(D_1 u + D_2 v + D_3 y + D_4 w)^{3+2\epsilon}}, \tag{9}$$

with $w=1-u-v-y$. The integration variables (u, v and y) run in the simplex S defined through $u,v,y\geqslant 0$ and $u+v+y\leqslant 1$. After the integration over r one simplifies the remaining integrals with the help of the substitutions

$$u\to(1-u')\left(1-\frac{1-v'}{u'}\right),\quad v\to\frac{1-u'}{u'}(1-v'),\quad y\to u'y'. \tag{10}$$

The integration variable v' varies in the interval $[1-u',1]$ whereas the other three variables x, y', and u' all vary in the interval $[0,1]$. We tighten the notation by omitting the primes and arrive at

$$M_{2,\mathrm{bare}}^{(2)}(2c) = \frac{1}{8\pi^2}\left(\frac{\alpha_s}{\pi}\right)^2 eQ_d C_F T n_f \frac{\Gamma(\epsilon)\Gamma^2(2-\epsilon)(1-\epsilon)}{\Gamma(4-2\epsilon)} \times e^{3\gamma_E\epsilon}\mu^{6\epsilon}\int_0^1 dx\int_0^1 dy\int_0^1 du \times\int_{1-u}^1 dv\, x^{1-\epsilon}(1-x)^{1-\epsilon}y^{\epsilon-1}(1-y)^{\epsilon} \times u^{2\epsilon-1}\overline{u}(p')\left(\frac{P_1}{\hat{C}^{1+3\epsilon}}+\frac{P_2}{\hat{C}^{3\epsilon}}+\frac{P_3\hat{C}}{\hat{C}^{3\epsilon}}\right)u(p), \tag{11}$$

where the Dirac matrices P_1, P_2, and P_3 are polynoms in the Feynman parameters and the expression $\hat{C}$ is given by

$$\hat{C}=m_b^2(1-u)v+\frac{uy}{x(1-x)}m_c^2-i\delta. \tag{12}$$

We should mention at this point that the expression in Eq. (11) is infrared finite and is therefore regularized for $\epsilon>0$.

We use the same approach as in Refs. [20,26,27] and introduce Mellin-Barnes representations for the denominators $\hat{C}^{1+3\epsilon}$ and $\hat{C}^{3\epsilon}$. In general the Mellin-Barnes representation of an expression of the form $(K^2-M^2)^{-\lambda}$ (with $\lambda>0$) reads

$$\frac{1}{(K^2-M^2)^{\lambda}} = \frac{1}{(K^2)^{\lambda}}\frac{1}{\Gamma(\lambda)}\frac{1}{2\pi i}\int_{\gamma} ds \times\left(-\frac{M^2}{K^2}\right)^s \Gamma(-s)\Gamma(\lambda+s), \tag{13}$$

where the integration path γ runs parallel to the imaginary axis. It intersects the real axis somewhere between $-\lambda$ and 0. The Mellin-Barnes representation for $\hat{C}^{\lambda}$, ($\lambda\in\{3\epsilon,1+3\epsilon\}$) is implemented by identifying K^2 and M^2 as

$$K^2\leftrightarrow m_b^2(1-u)v,$$
$$M^2\leftrightarrow -\frac{uy}{x(1-x)}m_c^2+i\delta. \tag{14}$$

The integration path γ has to be chosen such that the parameter integrals exist for all values of $s\in\gamma$. This means in our case that γ has to intersect the real s-axis between -3ϵ and 0. After interchanging the order of integration, the four Feynman parameter integrals can easily be expressed in terms of products of Euler Γ functions. What remains to be done is the integration over γ in the complex s plane. We close the integration path in the right half-plane and use the residue theorem to perform this integral. The residues are located at the following positions:

$$s=0,1,2,\ldots,$$

$$s=1-\epsilon,2-\epsilon,3-\epsilon,\ldots,$$

$$s=1-2\epsilon,2-2\epsilon,3-2\epsilon,\ldots,$$

$$s=1-3\epsilon,2-3\epsilon,3-3\epsilon,\ldots,$$

$$s=\frac{1}{2}-3\epsilon,\frac{3}{2}-3\epsilon,\frac{5}{2}-3\epsilon,\ldots. \tag{15}$$

The sum over the residues naturally leads to an expansion in the small parameter $z=m_c^2/m_b^2$ through the factor $(m_c^2/m_b^2)^s$ in Eq. (13) [see also Eq. (14)]. This expansion, however, is not a Taylor series because it also involves logarithms of z, which are generated by the expansion in ϵ. The final result for $M_{2,\mathrm{bare}}^{(2)}(2c)$ can thus be written as

$$M_{2,\mathrm{bare}}^{(2)}(2c)=\sum_{k,l} f_{k,l} z^k \ln^l(z), \tag{16}$$

where the coefficients $f_{k,l}$ are independent of z. The power k is an (non-negative) integer multiple of $\frac{1}{2}$ and $l \in \{0,1,2,3,4\}$. For a detailed explanation of the range of l we refer to Ref. [20].

In a similar way all other diagrams can be treated. The final result for the sum of the three-loop diagrams is given by

$$M_{2,\mathrm{bare}}^{(2)}=M_{2,\mathrm{bare}}^{(2)}(1)+M_{2,\mathrm{bare}}^{(2)}(2)+M_{2,\mathrm{bare}}^{(2)}(3)+M_{2,\mathrm{bare}}^{(2)}(4), \tag{17}$$

where the analytical results for the individual terms of the right-hand side are listed in Appendix B. We decided to include corrections up to $\mathcal{O}(z^3)$ as the higher order terms lead to a negligible contribution for the physical value $z\approx 0.1$.

B. Counterterm contributions to $\langle s\gamma|O_2|b\rangle$

In this section we work out the various counterterms of order $\alpha_s^2 n_f$ which are needed to derive the renormalized result $M_2^{(2)}$. There are counterterm contributions due to the renormalization of the strong coupling constant and due to the mixing of O_2 into other operators.

We first discuss the counterterms related to the renormalization of α_s. As the leading term $M_{2,\mathrm{bare}}^{(0)}$ is zero, only the renormalization of g_s in the two-loop result $M_{2,\mathrm{bare}}^{(1)}$ generates a counterterm which can be written as

$$M_{2,g_s}^{(2)}=2\,\delta Z_{g_s}^{(1),n_f} M_{2,\mathrm{bare}}^{(1)},$$

$$\delta Z_{g_s}^{(1),n_f}=\frac{\alpha_s}{\pi}\frac{n_f T}{6\epsilon}. \tag{18}$$

$M_{2,\mathrm{bare}}^{(1)}$ is the sum of the two-loop diagrams which has to be known including terms of $\mathcal{O}(\epsilon)$. For this reason we extended the calculation of Ref. [20] to order ϵ^1.

We now turn to the counterterms induced through the mixing of O_2 with other operators. First, we consider the counterterms connected with the mixing of O_2 into four-fermion operators. At order α_s there are nonvanishing mixings into O_1, O_4 and into the evanescent operator P_{11}, defined in Appendix A of Ref. [12]. As only O_4 has a nonvanishing matrix element for $b\to s\gamma$ proportional to $\alpha_s n_f$, the only counterterm of this type is

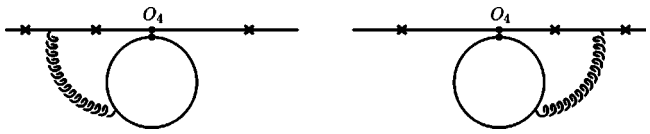

FIG. 3. Counterterm diagrams to O_2 involving the operator O_4. The crosses denote the possible places for photon emission. Note that the diagrams where the photon is emitted from the fermion-loop are zero due to Furry's theorem.

$$M_{24,a}^{(2)}=\delta Z_{24}^{(1)} M_4^{(1)},$$

$$\delta Z_{24}^{(1)}=\frac{\alpha_s}{\pi}\frac{1}{6\epsilon},$$

$$\begin{aligned} M_4^{(1)}=\frac{1}{81}\Bigg[&-\frac{72}{\epsilon}+78+288\ln\left(\frac{m_b}{\mu}\right)+36i\pi+1159\epsilon \\ &-150\pi^2\epsilon-312\ln\left(\frac{m_b}{\mu}\right)\epsilon-576\ln^2\left(\frac{m_b}{\mu}\right)\epsilon \\ &+258i\pi\epsilon-144i\pi\ln\left(\frac{m_b}{\mu}\right)\epsilon+\mathcal{O}(\epsilon^2)\Bigg]\frac{\alpha_s}{4\pi}C_F T n_f \\ &\times Q_d\langle s\gamma|O_7|b\rangle_{\mathrm{tree}}, \end{aligned} \tag{19}$$

where $\delta Z_{24}^{(1)}$ can be found in Ref. [12]. The Feynman diagrams contributing to $M_4^{(1)}$, i.e., to the corrections of $\mathcal{O}(\alpha_s n_f)$ to $\langle s\gamma|O_4|b\rangle_{\mathrm{tree}}$, are depicted in Fig. 3. They were computed following the strategy outlined in Sec. II A.

At order $\alpha_s^2 n_f$, there are mixings of O_2 into O_1, O_4, and P_{11} and again only O_4 has a matrix element of $\mathcal{O}(\alpha_s^0)$. Thus the only counterterm of this type reads

$$M_{24,b}^{(2)}=\delta Z_{24}^{(2),n_f} M_4^{(0)},$$

$$\delta Z_{24}^{(2),n_f}=\left(\frac{a_s}{\pi}\right)^2\frac{n_f T}{18\epsilon^2},$$

$$\begin{aligned} M_4^{(0)}=&\left[1-2\ln\left(\frac{m_b}{\mu}\right)\epsilon+\frac{\pi^2\epsilon^2}{12}+2\ln^2\left(\frac{m_b}{\mu}\right)\epsilon^2+\mathcal{O}(\epsilon^3)\right] \\ &\times C_F Q_d\langle s\gamma|O_7|b\rangle_{\mathrm{tree}}. \end{aligned} \tag{20}$$

In a second step we consider the counterterms connected with the mixing of O_2 into the dipole operators O_7 and O_8. One can easily see that only one counterterm of this type generates a contribution of $\mathcal{O}(\alpha_s^2 n_f)$: O_2 mixes at three-loop order into O_7; in turn, from O_7 the tree-level matrix element for $b\to s\gamma$ is taken. The resulting counterterm therefore reads [12,28]

$$M_{27}^{(2)} = \delta Z_{27}^{(2),n_f} \langle s\gamma|O_7|b\rangle_{\rm tree},$$

$$\delta Z_{27}^{(2),n_f} = \left(\frac{\alpha_s}{\pi}\right)^2 C_F T n_f \left[\frac{1}{\epsilon^2}\left(\frac{Q_u}{24}-\frac{Q_d}{81}\right)-\frac{1}{\epsilon}\left(\frac{Q_u}{144}+\frac{2Q_d}{243}\right)\right], \tag{21}$$

where $Q_u = 2/3$ and $Q_d = -1/3$ are the charge factors of up- and down-type quarks, respectively.

C. Renormalized result for $\langle s\gamma|O_2|b\rangle$

Combining the three-loop result $M_{2,\rm bare}^{(2)}$, calculated in Sec. II A, with the various counterterm contributions discussed in Sec. II B [see Eqs. (18), (19), (20), and (21)], we get an ultraviolet finite result. As mentioned earlier, the result is also free of infrared singularities. Inserting the numerical values for the color factors ($C_F = 4/3$, $T = 1/2$) and the electric charge factors ($Q_u = 2/3$, $Q_d = -1/3$), we get the following renormalized result:

$$\begin{aligned} M_2^{(2)} &= M_{2,\rm bare}^{(2)} + M_{2,g_s}^{(2)} + M_{24,a}^{(2)} + M_{24,b}^{(2)} + M_{27}^{(2)} \\ &= \left(\frac{\alpha_s}{4\pi}\right)^2 n_f \langle s\gamma|O_7|b\rangle_{\rm tree} \left[t_2^{(2)} \ln^2\left(\frac{m_b}{\mu}\right) + l_2^{(2)} \ln\left(\frac{m_b}{\mu}\right) + r_2^{(2)}\right], \end{aligned} \tag{22}$$

with

$$t_2^{(2)} = \frac{800}{243}, \tag{23}$$

$$\begin{aligned} \mathrm{Re}(l_2^{(2)}) = \frac{16}{243}[&-145 + (288 - 30\pi^2 - 216\zeta(3) + 216L - 54\pi^2 L + 18L^2 + 6L^3)z + 24\pi^2 z^{3/2} \\ &+ 6(18 + 2\pi^2 + 12L - 6\pi^2 L + L^3)z^2 - (9 + 14\pi^2 - 182L + 126L^2)z^3] + \mathcal{O}(z^4), \end{aligned} \tag{24}$$

$$\mathrm{Im}(l_2^{(2)}) = \frac{16\pi}{243}[-22 + (180 - 12\pi^2 + 36L + 36L^2)z - (12\pi^2 - 36L^2)z^2 + (112 - 48L)z^3] + \mathcal{O}(z^4), \tag{25}$$

$$\begin{aligned} \mathrm{Re}(r_2^{(2)}) = \frac{67454}{6561} - \frac{124\pi^2}{729} - \frac{4}{1215}&(11280 - 1520\pi^2 - 171\pi^4 - 5760\zeta(3) + 6840L - 1440\pi^2 L - 2520\zeta(3)L + 120L^2 \\ &+ 100L^3 - 30L^4)z - \frac{64\pi^2}{243}[43 - 12\ln(2) - 3L]z^{3/2} - \frac{2}{1215}[11475 - 380\pi^2 + 96\pi^4 + 7200\zeta(3) - 1110L \\ &- 1560\pi^2 L + 1440\zeta(3)L + 990L^2 + 260L^3 - 60L^4]z^2 + \frac{2240\pi^2}{243}z^{5/2} - \frac{2}{2187}[62471 - 2424\pi^2 - 33264\zeta(3) \\ &- 19494L - 504\pi^2 L - 5184L^2 + 2160L^3]z^3 + \mathcal{O}(z^{7/2}), \end{aligned} \tag{26}$$

$$\begin{aligned} \mathrm{Im}(r_2^{(2)}) = \frac{4\pi}{729}\{&495 - 12[375 - 19\pi^2 + 36\zeta(3) + 84L + 48L^2 - 6L^3]z + 6[207 + 38\pi^2 - 72\zeta(3) - 126L - 78L^2 + 12L^3]z^2 \\ &+ 8(67 - 12\pi^2 - 48L)z^3\} + \mathcal{O}(z^4), \end{aligned} \tag{27}$$

where $L = \ln z$. We note that in the derivation of this $\mathcal{O}(\alpha_s^2 n_f)$ result, there was no need to renormalize the parameter m_b in the corresponding $\mathcal{O}(\alpha_s^1)$ expression. Therefore, the symbol $\langle s\gamma|O_7|b\rangle_{\rm tree}$ can be interpreted to be (in $M_2^{(1)}$ and $M_2^{(2)}$)

$$\langle s\gamma|O_7|b\rangle_{\rm tree} = m_b \frac{e}{8\pi^2}\bar{u}(p')\not{\epsilon}\not{q}u(p), \tag{28}$$

where m_b denotes the pole mass of the b quark. Concerning this point, the reader is also referred to Sec. III.

We now turn to the renormalized matrix element $M_1^{(2)}$, associated with the operator O_1. O_1, defined in Eq. (4), can be written as

$$O_1 = \frac{1}{2}\tilde{O}_1 - \frac{1}{6}O_2, \tag{29}$$

with

$$\tilde{O}_1 = (\bar{s}_L^\alpha \gamma_\mu c_L^\beta)(\bar{c}_L^\beta \gamma^\mu b_L^\alpha), \tag{30}$$

where α and β are color indices. It is easy to see that $\tilde{O}_1$ has a vanishing matrix element for $b \to s\gamma$. Therefore, one obtains

$$M_1^{(2)} = -\frac{1}{6}M_2^{(2)}. \tag{31}$$

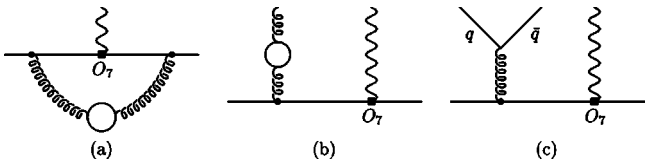

FIG. 4. Virtual (a), gluon-bremsstrahlung (b), and quark-pair radiation (c) graphs to the operator O_7. In (b) and (c), the diagrams where the gluon is emitted from the s quark are not shown.

III. REAL AND VIRTUAL CORRECTIONS TO $\langle s\gamma|O_7|b\rangle$

In this section we describe in some detail the steps needed for the calculation of the $\mathcal{O}(\alpha_s^2 n_f)$ corrections to the matrix element $\langle s\gamma|O_7|b\rangle$. Due to the presence of infrared singularities, the practical calculation proceeds in a slightly different way than for O_2. As these singularities only get canceled at the level of the decay width when combining the virtual corrections shown in Fig. 4(a) with the gluon bremsstrahlung [Fig. 4(b)] and the quark-pair emission process [Fig. 4(c)], we first derive expressions for the $\mathcal{O}(\alpha_s^2 n_f)$ corrections to these three contributions to the decay width. The corresponding expressions necessary to evaluate $\mathrm{BR}(B\to X_s\gamma)_{E_\gamma\geqslant E_{\rm cut}}$ are discussed in Appendix E.

To fix the notation, we write the contribution from O_7 to the decay width $\Gamma(b\to X_s\gamma)$ as

$$\Gamma_{77}=\Gamma_{77}^0[1+\hat\Gamma_{77}^{(1)}+\hat\Gamma_{77}^{(2),n_f}],\quad \Gamma_{77}^0=\frac{m_b^5\alpha_{\rm em}}{32\pi^4}|G_F\lambda_t C_7^{\rm eff}|^2. \tag{32}$$

The $\mathcal{O}(\alpha_s)$ correction $\hat\Gamma_{77}^{(1)}$ can be extracted from Ref. [20], reading

$$\hat\Gamma_{77}^{(1)}=\frac{\alpha_s}{4\pi}\left[-\frac{32}{9}-\frac{16\pi^2}{9}+\frac{64}{3}\ln\left(\frac{m_b}{\mu}\right)\right]. \tag{33}$$

We further split $\hat\Gamma_{77}^{(2),n_f}$ in Eq. (32) as

$$\hat\Gamma_{77}^{(2),n_f}=\hat\Gamma_{77}^{(2),(a)}+\hat\Gamma_{77}^{(2),(b)}+\hat\Gamma_{77}^{(2),(c)}, \tag{34}$$

with obvious notation (Fig. 4).

For the calculation of the three parts contributing to $\hat\Gamma_{77}^{(2),n_f}$ we could in principle put $m_f=m_s=0$ at the beginning of the calculation and use dimensional regularization for both infrared and ultraviolet singularities. We found it easier, however, to use the strange quark mass m_s and the mass of the quark in the fermion bubble m_f as infrared regulators. For formulating the results, it is convenient to introduce the dimensionless quantities

$$r=\frac{m_s^2}{m_b^2},\quad f=\frac{m_f^2}{m_b^2}. \tag{35}$$

We now turn to the calculations of $\hat\Gamma_{77}^{(2),(c)}$, $\hat\Gamma_{77}^{(2),(b)}$, and $\hat\Gamma_{77}^{(2),(a)}$ (in this order).

Inspecting the explicit expressions for the quark-pair radiation process [cf. Fig. 4(c)], one finds that it can be worked out in our ''massive'' regularization scheme in $d=4$ dimensions. Furthermore, one realizes that one can also put $m_s=0$, provided m_f is kept at a (small) fixed value. As a consequence, the quark-pair radiation process is completely regularized by the mass m_f. The evaluation of this process is quite standard: in a first step the subprocess $b\to s\gamma g^\star$ is considered where $g^\star$ represents a virtual gluon. Subsequently the other subprocess, describing the decay of $g^\star$ into two fermions, is added. It is straightforward to perform the occurring phase space integrations where only the one over the gluon virtuality is nontrivial. However, in the limit $m_f\to 0$ also this one can be performed analytically. One arrives at the following result for the quark-pair emission process:

$$\hat\Gamma_{77}^{(2),(c)}=\left(\frac{\alpha_s}{4\pi}\right)^2\frac{n_f}{243}[-12662+24\pi^2+2592\zeta(3)+(144\pi^2-5916)\ln(f)-900\ln^2(f)-72\ln^3(f)]. \tag{36}$$

Due to the Kinoshita-Lee-Nauenberg theorem, it follows that the sum of the virtual and the gluon bremsstrahlung corrections also must be finite for $d\to 4$ and $m_s\to 0$ for fixed m_f.

We now turn to the gluon bremsstrahlung process. The diagram in Fig. 4(b) (combined with the one where the gluon is emitted from the s quark) can be written as

$$M_{7,\rm bare}^{(2),(b)}=\frac{\delta Z_3^{(1),n_f}}{2}M_7^{(1),(b)}, \tag{37}$$

where $M_7^{(1),(b)}$ denotes the lowest order matrix element for $b\to s\gamma g$ and $\delta Z_3^{(1),n_f}$ reads

$$\delta Z_3^{(1),n_f}=-\frac{\alpha_s}{\pi}\frac{n_f T}{36}\left[\frac{12}{\epsilon}-24\ln\left(\frac{m_f}{\mu}\right)+\pi^2\epsilon+24\ln^2\left(\frac{m_f}{\mu}\right)\epsilon+\mathcal{O}(\epsilon^2)\right]. \tag{38}$$

Note that the $1/\epsilon$ pole is of ultraviolet origin; the infrared singularity is regulated by m_f in this expression. In addition, there is a counterterm contribution due to the $\overline{\rm MS}$ renormalization of the strong coupling constant of the form

$$M_{7,\rm ct}^{(2),(b)}=\delta Z_{g_s}^{(1),n_f}M_7^{(1),(b)}, \tag{39}$$

with

$$\delta Z_{g_s}^{(1),n_f}=\frac{\alpha_s}{\pi}\frac{n_f T}{6\epsilon}. \tag{40}$$

Combining $M_{7,\rm bare}^{(2),(b)}$ with $M_{7,\rm ct}^{(2),(b)}$, one obtains the renormalized matrix element $M_7^{(2),(b)}$

$$M_7^{(2),(b)}=\left(\delta Z_{g_s}^{(1),n_f}+\frac{\delta Z_3^{(1),n_f}}{2}\right)M_7^{(1),(b)}, \tag{41}$$

from which the $\mathcal{O}(\alpha_s^2 n_f)$ contribution to the decay width is obtained in a straightforward way. One gets

$$\hat{\Gamma}_{77}^{(2),(b)} = 2\left(\delta Z_{g_s}^{(1),n_f} + \frac{\delta Z_3^{(1),n_f}}{2}\right)\hat{\Gamma}_{77}^{(1),(b)}$$

$$= \left(\frac{\alpha_s}{4\pi}\right)^2 C_F T n_f \left\{\frac{48}{\epsilon}\left[2\ln(f) + 4\ln\left(\frac{m_b}{\mu}\right) + \ln(f)\ln(r) + 2\ln\left(\frac{m_b}{\mu}\right)\ln(r)\right] - 8\pi^2 + 416\ln(f) - 32\pi^2\ln(f) - 48\ln^2(f)\right.$$

$$+ 832\ln\left(\frac{m_b}{\mu}\right) - 64\pi^2\ln\left(\frac{m_b}{\mu}\right) - 960\ln^2\left(\frac{m_b}{\mu}\right) - 576\ln(f)\ln\left(\frac{m_b}{\mu}\right) - 4\ln(r)\left[\pi^2 - 18\ln(f) + 6\ln^2(f) - 36\ln\left(\frac{m_b}{\mu}\right)\right.$$

$$\left.\left. + 120\ln^2\left(\frac{m_b}{\mu}\right) + 72\ln(f)\ln\left(\frac{m_b}{\mu}\right)\right] - 24\ln^2(r)\left[\ln(f) + 2\ln\left(\frac{m_b}{\mu}\right)\right]\right\}, \tag{42}$$

where $\hat{\Gamma}_{77}^{(1),(b)}$ is the corresponding (normalized) decay width for $b \to s\gamma g$ in the $\mathcal{O}(\alpha_s)$ approximation. As in our regularization scheme the sum $\delta Z_{g_s}^{(1),n_f} + \delta Z_3^{(1),n_f}/2$ is finite (in ϵ), $\hat{\Gamma}_{77}^{(1),(b)}$ is only needed up to terms of order ϵ^0, which simplified the calculation.

We now turn to the evaluation of the virtual corrections shown in Fig. 4(a) and also discuss the various counterterm contributions. For the diagram shown in this figure, we obtain

$$M_{7,\mathrm{bare}}^{(2),(a)} = \frac{1}{81}\left\{\frac{54}{\epsilon^2}(2\ln(r) - 1) + \frac{18}{\epsilon}\left[2 + 12\ln(r) - 6\ln(r)\ln(f) - 24\ln(r)\ln\left(\frac{m_b}{\mu}\right) - 3\ln^2(r) + 6\ln(f) + 12\ln\left(\frac{m_b}{\mu}\right)\right] + 1718\right.$$

$$+ 123\pi^2 + 840\ln(f) + 36\pi^2\ln(f) + 90\ln^2(f) + 18\ln^3(f) - 144\ln\left(\frac{m_b}{\mu}\right) - 432\ln^2\left(\frac{m_b}{\mu}\right) - 432\ln(f)\ln\left(\frac{m_b}{\mu}\right)$$

$$+ 18\ln(r)\left[24 + \pi^2 - 12\ln(f) + 3\ln^2(f) - 48\ln\left(\frac{m_b}{\mu}\right) + 48\ln^2\left(\frac{m_b}{\mu}\right) + 24\ln(f)\ln\left(\frac{m_b}{\mu}\right)\right]$$

$$\left. - 54\ln^2(r)\left[2 - \ln(f) - 4\ln\left(\frac{m_b}{\mu}\right)\right] + 18\ln^3(r)\right\}\left(\frac{\alpha_s}{4\pi}\right)^2 C_F T n_f \langle s\gamma|O_7|b\rangle_{\mathrm{tree}}. \tag{43}$$

We stress that this expression is derived in such a way that m_s is understood to be sent to zero prior to m_f. This procedure is justified by the fact that for fixed m_f the sum of the virtual and gluon bremsstrahlung contributions must be finite in the limit $m_s \to 0$, as discussed above.

The counterterm contribution $M_{7,\mathrm{ct}}^{(2),(a)}$ at $\mathcal{O}(\alpha_s^2 n_f)$ has various sources. There is a contribution $M_{7,\mathrm{ct}_1}^{(2),(a)}$ due to the renormalization of g_s in the $\mathcal{O}(\alpha_s)$ vertex diagram [i.e., similar to the one in Fig. 4(a), but without the fermion bubble], yielding

$$M_{7,\mathrm{ct}_1}^{(2),(a)} = \frac{1}{9}\left\{-\frac{12}{\epsilon^2}\ln(r) - \frac{6}{\epsilon}\ln(r)\left[4 - \ln(r) - 4\ln\left(\frac{m_b}{\mu}\right)\right]\right.$$

$$+ 12 - \ln(r)\left[48 + \pi^2 - 48\ln\left(\frac{m_b}{\mu}\right) + 24\ln^2\left(\frac{m_b}{\mu}\right)\right]$$

$$\left. + 12\ln^2(r)\left[1 - \ln\left(\frac{m_b}{\mu}\right)\right] - 2\ln^3(r)\right\}$$

$$\times\left(\frac{\alpha_s}{4\pi}\right)^2 C_F T n_f \langle s\gamma|O_7|b\rangle_{\mathrm{tree}}. \tag{44}$$

Then, there is a counterterm contribution $M_{7,\mathrm{ct}_2}^{(2),(a)}$ of the form

$$M_{7,\mathrm{ct}_2}^{(2),(a)} = \left(\frac{\delta Z_{2,b}^{(2),n_f}}{2} + \frac{\delta Z_{2,s}^{(2),n_f}}{2} + \delta Z_{77}^{(2),n_f} + \delta Z_{m_b}^{\mathrm{on},(2),n_f}\right)$$

$$\times\langle s\gamma|O_7|b\rangle_{\mathrm{tree}}. \tag{45}$$

Here, $\delta Z_{2,b}^{(2),n_f}$ and $\delta Z_{2,s}^{(2),n_f}$ are the $\mathcal{O}(\alpha_s^2 n_f)$ pieces of the on-shell wave function renormalization constants for the b and s quark, respectively, while the operator renormalization factor $\delta Z_{77}^{(2),n_f}$ refers to the $\overline{\mathrm{MS}}$ scheme. Note that the presence of the *on-shell* renormalization factor $\delta Z_{m_b}^{\mathrm{on},(2),n_f}$ in Eq. (45) implies that in the lower order contributions the symbol $\langle s\gamma|O_7|b\rangle_{\mathrm{tree}}$ is understood to be the tree-level matrix element of O_7 in which the running b-quark mass is replaced by the corresponding pole mass. The explicit form of the various δZ factors occurring in Eq. (45) can be seen in Appendix D.

After combining Eqs. (43), (44), and (45) into the renormalized matrix element, the calculation of $\hat{\Gamma}_{77}^{(2),(a)}$ is straightforward. We obtain

$$\hat{\Gamma}_{77}^{(2),(a)}=\left(\frac{\alpha_s}{4\pi}\right)^2\frac{C_F T n_f}{81}\left\{\frac{-216}{\epsilon}\left[2\ln(f)+4\ln\left(\frac{m_b}{\mu}\right)+\ln(f)\ln(r)+2\ln\left(\frac{m_b}{\mu}\right)\ln(r)\right]+7495+624\pi^2+1086\ln(f)\right.$$
$$+72\pi^2\ln(f)+666\ln^2(f)+36\ln^3(f)-6336\ln\left(\frac{m_b}{\mu}\right)+6048\ln^2\left(\frac{m_b}{\mu}\right)+2592\ln(f)\ln\left(\frac{m_b}{\mu}\right)+18\ln(r)\left[\pi^2-18\ln(f)\right.$$
$$\left.\left.+6\ln^2(f)-36\ln\left(\frac{m_b}{\mu}\right)+120\ln^2\left(\frac{m_b}{\mu}\right)+72\ln(f)\ln\left(\frac{m_b}{\mu}\right)\right]+108\ln^2(r)\left[\ln(f)+2\ln\left(\frac{m_b}{\mu}\right)\right]\right\}. \quad (46)$$

We now combine virtual and gluon bremsstrahlung corrections given in Eqs. (46) and (42), respectively. We obtain (after putting $T=1/2$ and $C_F=4/3$)

$$\hat{\Gamma}_{77}^{(2),(a)+(b)}=\left(\frac{\alpha_s}{4\pi}\right)^2\frac{n_f}{243}\left[14990+1176\pi^2+(5916-144\pi^2)\right.$$
$$\times\ln(f)+900\ln^2(f)+72\ln^3(f)-576(9+\pi^2)$$
$$\left.\times\ln\left(\frac{m_b}{\mu}\right)+3456\ln^2\left(\frac{m_b}{\mu}\right)\right], \quad (47)$$

where the $1/\epsilon$ poles and the mass singularities associated with m_s are canceled.

When combining this result with the quark-pair emission process in Eq. (36), we obtain the final result

$$\hat{\Gamma}_{77}^{(2),n_f}=\left[\frac{\alpha_s}{4\pi}\right]^2 n_f\left[2t_7^{(2)}\ln^2\left(\frac{m_b}{\mu}\right)+2l_7^{(2)}\ln\left(\frac{m_b}{\mu}\right)+2r_7^{(2)}\right], \quad (48)$$

with

$$t_7^{(2)}=\frac{64}{9},$$

$$l_7^{(2)}=-\frac{32}{27}(9+\pi^2),$$

$$r_7^{(2)}=\frac{4}{81}[97+50\pi^2+108\zeta(3)]. \quad (49)$$

The cancellation of the $\ln(f)$ terms is a strong check for the correctness of the individual pieces of the calculation.

For later convenience we formally introduce an amplitude M_7 in such a way that its square reproduces the result of Eq. (48). Adopting the notation of Eq. (6) one gets

$$M_7^{(2)}=\left(\frac{\alpha_s}{4\pi}\right)^2 n_f\langle s\gamma|O_7|b\rangle_{\rm tree}\left[t_7^{(2)}\ln^2\left(\frac{m_b}{\mu}\right)\right.$$
$$\left.+l_7^{(2)}\ln\left(\frac{m_b}{\mu}\right)+r_7^{(2)}\right]. \quad (50)$$

IV. VIRTUAL CORRECTIONS TO $\langle s\gamma|O_8|b\rangle$

We first discuss the two-loop diagrams depicted in Fig. 5, which contain the building block $K^f_{\beta\beta'}$ [see Eq. (A2)]. As these diagrams are free of infrared singularities, we put the masses m_f of the quarks in the fermion loop as well as the strange quark mass m_s to zero from the beginning. The calculation can be performed along the same lines as described in Sec. II A. However, due to the absence of m_c, the actual evaluation of the diagrams turns out to be much simpler. The result can be cast into the form

$$M_{8,\rm bare}^{(2)}=\left(\frac{\alpha_s}{4\pi}\right)^2 C_F T n_f Q_d\langle s\gamma|O_7|b\rangle_{\rm tree}\frac{4}{27}$$
$$\times\left[\left(\frac{18}{\epsilon^2}+\frac{1}{\epsilon}(120-6\pi^2+18i\pi)\right)\left(\frac{m_b}{\mu}\right)^{-4\epsilon}\right.$$
$$\left.+530-28\pi^2-180\zeta(3)+93i\pi\right]. \quad (51)$$

The counterterm contribution of $\mathcal{O}(\alpha_s^2 n_f)$, denoted by $M_{8,\rm ct}^{(2)}$, stems from the renormalization of g_s and from the mixing of O_8 into the operator O_7. We obtain

$$M_{8,\rm ct}^{(2)}=\delta Z_{87}^{(2),n_f}\langle s\gamma|O_7|b\rangle_{\rm tree}+2\,\delta Z_{g_s}^{(1),n_f}M_8^{(1)}, \quad (52)$$

with

$$\delta Z_{87}^{(2),n_f}=\left(\frac{\alpha_s}{\pi}\right)^2 C_F T n_f\frac{Q_d}{36\epsilon}\left(\frac{6}{\epsilon}-7\right),$$

$$\delta Z_{g_s}^{(1),n_f}=\frac{\alpha_s}{\pi}\frac{n_f T}{6\epsilon},$$

$$M_8^{(1)}=-\frac{\alpha_s}{4\pi}\frac{1}{3}Q_d C_F\langle s\gamma|O_7|b\rangle_{\rm tree}\left\{\frac{12}{\epsilon}+33-2\pi^2\right.$$
$$-24\ln\left(\frac{m_b}{\mu}\right)+6i\pi+\epsilon\left[72-4\pi^2-36\zeta(3)\right.$$
$$-66\ln\left(\frac{m_b}{\mu}\right)+4\pi^2\ln\left(\frac{m_b}{\mu}\right)+24\ln^2\left(\frac{m_b}{\mu}\right)$$
$$\left.\left.+12i\pi-12i\pi\ln\left(\frac{m_b}{\mu}\right)\right]+\mathcal{O}(\epsilon^2)\right\}. \quad (53)$$

$\delta Z_{87}^{(2),n_f}$ is obtained from Refs. [12,28]. The sum of $M_{8,\rm bare}^{(2)}$ and $M_{8,\rm ct}^{(2)}$ leads to the renormalized result (using $T=1/2$, $C_F=4/3$ and $Q_d=-1/3$)

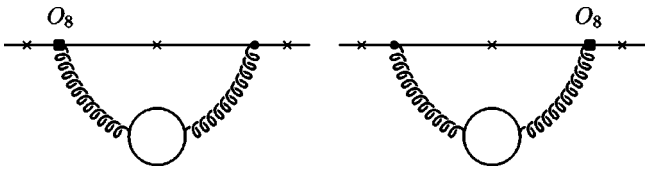

FIG. 5. Graphs associated with virtual corrections to the operator O_8. The crosses denote the possible places where the photon can be emitted.

$$M_8^{(2)}=\left(\frac{\alpha_s}{4\pi}\right)^2 n_f\langle s\gamma|O_7|b\rangle_{\rm tree}\left[t_8^{(2)}\ln^2\left(\frac{m_b}{\mu}\right)+l_8^{(2)}\ln\left(\frac{m_b}{\mu}\right)+r_8^{(2)}\right], \tag{54}$$

with

$$t_8^{(2)}=-\frac{64}{27},$$

$$l_8^{(2)}=\frac{16}{81}(47-2\pi^2+6i\pi),$$

$$r_8^{(2)}=\frac{8}{243}[-314+16\pi^2+72\zeta(3)-57i\pi]. \tag{55}$$

V. NUMERICAL IMPACT OF THE $\mathcal{O}(\alpha_s^2 n_f)$ CORRECTIONS

It is well known that the inclusive decay rate for $B\to X_s\gamma$ is given by the corresponding b-quark decay rate $\Gamma(b\to X_s\gamma)$, up to power corrections of the form $(\Lambda_{\rm QCD}/m_b)^2$ [29] and $(\Lambda_{\rm QCD}/m_c)^2$ [30] which numerically are well below 10%. As our new results are only a part of the complete NNLL contributions, we do not present a new prediction of the branching ratio in this paper. Instead, we only illustrate how the $\mathcal{O}(\alpha_s^2 n_f)$ corrections to the matrix elements of the operators O_1, O_2, O_7, and O_8 modify the NLL branching ratio for a given set of input parameters. For this purpose, we neglect power corrections and also electroweak terms.

In a NLL calculation the inclusive quark-level transition $b\to X_s\gamma$ involves the subprocesses $b\to s\gamma$ (including virtual corrections) and $b\to s\gamma g$, i.e., the gluon bremsstrahlung process. We write the amplitude for the first subprocess as in Ref. [14]:

$$\mathcal{A}^{\rm NLL}(b\to s\gamma)=-\frac{4G_F}{\sqrt{2}}V_{ts}^*V_{tb}D^{\rm NLL}\langle s\gamma|O_7|b\rangle_{\rm tree}, \tag{56}$$

where the reduced amplitude $D^{\rm NLL}$ reads

$$D^{\rm NLL}=C_7^{\rm eff}(\mu)+\frac{\alpha_s(\mu)}{4\pi}V^{(1)}(\mu). \tag{57}$$

The symbol $V^{(1)}(\mu)$, defined as

$$V^{(1)}(\mu)=\sum_{i=1}^{8}C_i^{\rm eff}(\mu)\left[\left(r_i^{(1)}-\frac{16}{3}\delta_{i7}\right)+(l_i^{(1)}+8\delta_{i7})\ln\left(\frac{m_b}{\mu}\right)\right], \tag{58}$$

incorporates the NLL corrections $r_i^{(1)}$ and $l_i^{(1)}$ to the matrix elements. In Eq. (57), the first term on the right-hand side is understood to be the Wilson coefficient $C_7^{\rm eff}(\mu)$ at NLL order, while the Wilson coefficients appearing in $V^{(1)}(\mu)$ are understood to be taken at LL order. As in Ref. [14], we convert the running mass factor $\overline{m}_b(\mu)$, which appears in the definition of the operator O_7 in Eq. (4), into the pole mass m_b. This conversion is absorbed into the function $V^{(1)}(\mu)$ and consequently the symbol $\langle s\gamma|O_7|b\rangle_{\rm tree}$ in Eq. (56) is the tree-level matrix element of the operator O_7, where the running mass factor $\overline{m}_b(\mu)$ is understood to be replaced by the pole mass m_b. The NLL virtual correction functions $r_i^{(1)}$ and $l_i^{(1)}$ in Eq. (58), taken from Ref. [20], are repeated for completeness in Appendix C. Note, that the quantity $r_7^{(1)}$ not only contains virtual corrections to the matrix element of O_7, which would be infrared singular. $r_7^{(1)}$ is constructed in such a way, that the (O_7,O_7) interference term generates the sum of virtual and bremsstrahlung corrections when formally calculating the branching ratio from $\mathcal{A}^{\rm NLL}(b\to s\gamma)$. For the details of this construction, we refer to Ref. [20]. Numerically, the square of this amplitude encodes the bulk of the decay width. The additional bremsstrahlung corrections, which are infrared finite for $E_{\rm gluon}\to 0$, are relatively small. Therefore, when considering terms of order $\mathcal{O}(\alpha_s^2 n_f)$, we omit purely finite bremsstrahlung contributions.

When improving the amplitude for the subprocess $b\to s\gamma$ by including the terms of $\mathcal{O}(\alpha_s^2 n_f)$, the result can be written as

$$\mathcal{A}(b\to s\gamma)=-\frac{4G_F}{\sqrt{2}}V_{ts}^*V_{tb}D\langle s\gamma|O_7|b\rangle_{\rm tree}, \tag{59}$$

where the reduced amplitude D is

$$D=C_7^{\rm eff}(\mu)+\frac{\alpha_s(\mu)}{4\pi}V^{(1)}(\mu)+\left(\frac{\alpha_s(\mu)}{4\pi}\right)^2 n_f V^{(2)}(\mu). \tag{60}$$

$V^{(2)}(\mu)$, defined as

$$V^{(2)}(\mu)=\sum_{i=1}^{8}C_i^{\rm eff}(\mu)\left[r_i^{(2)}+l_i^{(2)}\ln\left(\frac{m_b}{\mu}\right)+t_i^{(2)}\ln^2\left(\frac{m_b}{\mu}\right)\right], \tag{61}$$

incorporates the $\mathcal{O}(\alpha_s^2 n_f)$ corrections to the matrix elements calculated in the previous sections of this paper. The explicit $C_7^{\rm eff}(\mu)$ term in Eq. (60) in principle stands for the NLL Wilson coefficient, supplemented by the n_f dependent NNLL contributions. As the latter are not known yet, we take this Wilson coefficient at NLL precision in the numerical evaluations. The Wilson coefficients entering $V^{(1)}(\mu)$ are in prin-

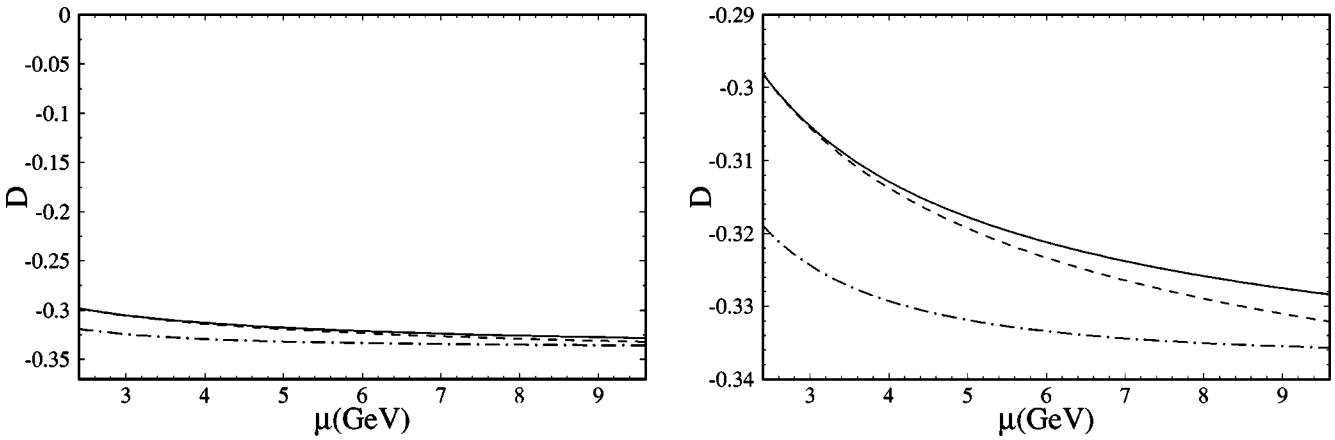

FIG. 6. The reduced amplitude D as a function of the renormalization scale μ where the plot on the right is an enlargement of the one on the left. The dash-dotted curve represents the NLL approximation and the solid curve includes the corrections of $\mathcal{O}(\alpha_s^2 n_f)$. For comparison we also show the result where the Wilson coefficients in $V^{(1)}$ [cf. Eq. (58)] are inserted to LL precision only (dashed curve).

ciple the LL coefficients, supplemented by the n_f dependent NLL contributions. In practice, we decide to replace these Wilson coefficients by the respective complete NLL version. Finally, the Wilson coefficients entering $V^{(2)}(\mu)$ are the LL versions. Note, that the gluon bremsstrahlung and the quark-antiquark emission processes associated with O_7 are effectively transferred into $r_7^{(2)}$, $l_7^{(2)}$, and $t_7^{(2)}$, as described in Sec. III. As already mentioned above, the square of the so-defined amplitude incorporates the major part of the branching ratio. We therefore consider the additional finite bremsstrahlung corrections to the decay width only at the NLL level, i.e., we do not calculate the $\mathcal{O}(\alpha_s^2 n_f)$ corrections to these contributions.

As the square of the amplitude for $b \to s\gamma$ (in the sense defined above) encodes the dominant part of the decay width, it is reasonable to compare the NLL result $D^{\rm NLL}$ in Eq. (57) with the corresponding $\mathcal{O}(\alpha_s^2 n_f)$-improved result D in Eq. (60). In Fig. 6, the function D is plotted as a function of the renormalization scale μ. We note, as already discussed in the Introduction, that we use in the numerical evaluations the hypothesis of naive non-Abelianization, which amounts to replacing n_f by $-3\beta_0/2$. Nevertheless, in the following we still write $\mathcal{O}(\alpha_s^2 n_f)$. The dash-dotted line shows the NLL approximation as defined in Eq. (57), while the solid curve shows the result after including the $\mathcal{O}(\alpha_s^2 n_f)$ terms as discussed above. The dashed line shows the result with $\mathcal{O}(\alpha_s^2 n_f)$ improvements, in which, however, the Wilson coefficients in $V^{(1)}(\mu)$ are taken in LL approximation. The three curves illustrate that the changes between the $\mathcal{O}(\alpha_s^2 n_f)$ improved version (solid line) and the NLL prediction (dash-dotted line) are mainly due to the new $\mathcal{O}(\alpha_s^2 n_f)$ corrections of the matrix elements calculated in the previous sections.

From $\mathcal{A}(b \to s\gamma)$ in Eq. (59) the decay width $\Gamma(b \to s\gamma)$ is easily obtained to be

$$\Gamma(b \to s\gamma) = \frac{G_F^2}{32\pi^4} |V_{ts}^* V_{tb}|^2 \alpha_{\rm em} m_b^5 |D|^2. \tag{62}$$

When giving numerical results for the NLL predictions, we only retain terms in $|D|^2$ up to order α_s, while for the improved version we retain terms up to $\mathcal{O}(\alpha_s^2 n_f)$ in $|D|^2$ and systematically dismiss higher order contributions. For completeness we should mention that $\alpha_s(\mu)$ is evaluated using two-loop accuracy in the β function. We checked that the contribution of the three-loop term β_2 is numerically small.

To obtain the inclusive decay rate for $b \to X_s\gamma$, we have to take into account those terms which have not yet been absorbed into the virtual corrections. At NLL precision, these contributions consist of those gluon bremsstrahlung corrections which are finite when the gluon energy goes to zero; they have been calculated in Refs. [31,32]. As the (O_8, O_8) contribution to $\Gamma(b \to s\gamma g)$ becomes infrared singular for *soft photon energies*, we introduce a photon energy cutoff $E_{\rm cut}$ as in Ref. [12] and define the kinematical decay width

$$\Gamma(b \to X_s\gamma)_{E_\gamma \geqslant E_{\rm cut}}. \tag{63}$$

At NLL the gluon bremsstrahlung contribution to this quantity can be written as

$$\Gamma(b \to s\gamma g)_{E_\gamma \geqslant E_{\rm cut}} = \frac{G_F^2}{32\pi^4} |V_{ts}^* V_{tb}|^2 \alpha_{\rm em} m_b^5 A, \tag{64}$$

where A is of the form [12]

$$A = (e^{-\alpha_s(\mu)\ln(\delta)[7+2\ln(\delta)]/(3\pi)} - 1) + \frac{\alpha_s(\mu)}{\pi} \sum_{i,j=1;i\leqslant j}^{8} {\rm Re}[C_i^{\rm eff}(\mu) C_j^{\rm eff}(\mu) f_{ij}(\delta)]. \tag{65}$$

The quantity δ is defined through

$$E_{\rm cut} = \frac{m_b}{2}(1-\delta) = E_{\rm max}(1-\delta). \tag{66}$$

In Eq. (65) we put $C_i^{\rm eff} = 0$ for $i = 3, \ldots, 6$, as in the virtual contributions. We list the explicit expressions for the quantities $f_{ij}(\delta)$ in Appendix C.

We should repeat that the $\mathcal{O}(\alpha_s^2 n_f)$ corrections are incorporated in the quantity D, defined in Eqs. (59) and (60). We

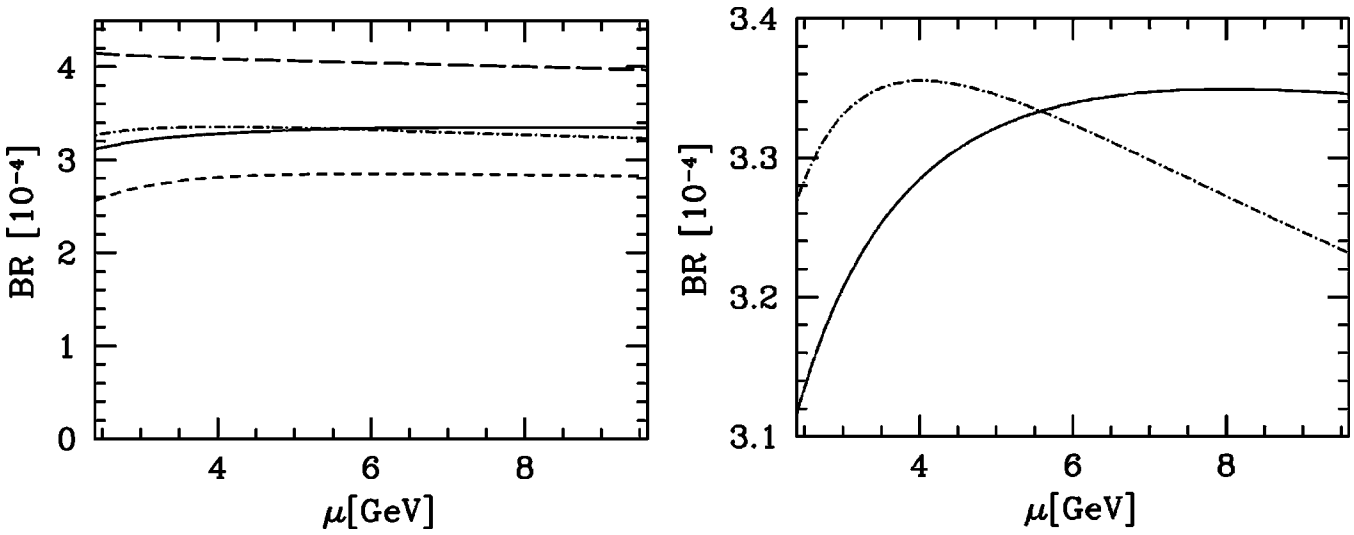

FIG. 7. The branching ratio as a function of the renormalization scale μ where the plot on the right is an enlargement of the one on the left. The dash-dotted curve represents the NLL approximation and the solid curve includes the corrections of $\mathcal{O}(\alpha_s^2 n_f)$. For illustration in the left plot the latter are also shown for the case where $M_{1/2}^{(2)}$ ($M_7^{(2)}$) is set to zero which corresponds to short-dashed (long-dashed) curve. A photon energy cut of $E_{\rm cut}=m_b/20$ is used, which corresponds to $\delta=0.9$.

stress that the absorbed gluon bremsstrahlung- and the quark-pair emission terms were obtained by integrating over the full range of the photon energy. Thus, since we decided to implement a photon energy cut as just described, the final expression for the kinematical decay width can be written as

$$\Gamma(b\to X_s\gamma)_{E_\gamma\geq E_{\rm cut}}=\frac{G_F^2}{32\pi^4}|V_{ts}^*V_{tb}|^2\alpha_{\rm em}m_b^5(|D|^2+A) - \Gamma_{77}^{(2),n_f}(b\to X_s\gamma)_{E_\gamma\leq E_{\rm cut}}, \quad (67)$$

where the expression for $\Gamma_{77}^{(2),n_f}(b\to X_s\gamma)_{E_\gamma\leq E_{\rm cut}}$ is derived in Appendix E.

In a last step, the kinematical branching ratio is obtained as

$$\mathrm{BR}(b\to X_s\gamma)_{E_\gamma\geq E_{\rm cut}}=\frac{\Gamma(b\to X_s\gamma)_{E_\gamma\geq E_{\rm cut}}}{\Gamma_{\rm SL}}\mathrm{BR}_{\rm SL}, \quad (68)$$

where $\mathrm{BR}_{\rm SL}$ is the measured semileptonic branching ratio and the semileptonic decay width $\Gamma_{\rm SL}$ [supplemented by the $\mathcal{O}(\alpha_s^2 n_f)$ terms [23]] is given by ($z=m_c^2/m_b^2$)

$$\Gamma_{\rm SL}=\frac{G_F^2|V_{cb}|^2m_b^5}{192\pi^3}g(z)\left\{1-\frac{2\alpha_s(\mu)}{3\pi}\frac{h(z)}{g(z)} -\left(\frac{\alpha_s(\mu)}{\pi}\right)^2\beta_0\left[\chi_\beta\left(\frac{m_c}{m_b}\right)-\frac{1}{3}\frac{h(z)}{g(z)}\ln\left(\frac{m_b}{\mu}\right)\right]\right\}, \quad (69)$$

where the phase space function $g(z)$ and the $\mathcal{O}(\alpha_s)$ radiation function $h(z)$ [33] read

$$g(z)=1-8z+8z^3-z^4-12z^2\ln(z),$$

$$h(z)=-(1-z^2)\left(\frac{25}{4}-\frac{239}{3}z+\frac{25}{4}z^2\right) +z\ln(z)\left(20+90z-\frac{4}{3}z^2+\frac{17}{3}z^3\right)+z^2\ln^2(z)(36+z^2) +(1-z^2)\left(\frac{17}{3}-\frac{64}{3}z+\frac{17}{3}z^2\right)\ln(1-z) -4(1+30z^2+z^4)\ln(z)\ln(1-z)-(1+16z^2+z^4) \times[6\,\mathrm{Li}_2(z)-\pi^2]-32z^{3/2}(1+z)\left[\pi^2-4\,\mathrm{Li}_2(\sqrt{z}) +4\,\mathrm{Li}_2(-\sqrt{z})-2\ln(z)\ln\left(\frac{1-\sqrt{z}}{1+\sqrt{z}}\right)\right]. \quad (70)$$

The function $\chi_\beta(m_c/m_b)$, which encodes the $\mathcal{O}(\alpha_s^2 n_f)$ terms[2] is given in the form of a plot in Ref. [23]. For $m_c/m_b=0.29$, which is the default value in our paper, one finds $\chi_\beta(0.29)\approx 1.68$.

In Fig. 7 the kinematical branching ratio is shown for the choice $E_{\rm cut}=m_b/20$ or, equivalently, $\delta=0.9$ [8] as a function of the renormalization scale μ. The input parameters were chosen to be $m_b=4.8$ GeV, $m_c/m_b=0.29$, $m_t=173.8$ GeV, $m_W=80.41$ GeV, $m_Z=91.187$ GeV, $\alpha_s(m_Z)=0.119$, $\alpha_{\rm em}=1/137.036$, $|V_{ts}^*V_{tb}/V_{cb}|^2=0.95$, and $\mathrm{BR}_{\rm SL}=10.49\%$. The dash-dotted line shows the branching ratio $\mathrm{BR}(b\to X_s\gamma)$ in NLL precision. In this case the terms of $\mathcal{O}(\alpha_s^2\beta_0)$ are consistently omitted in the expression for $\Gamma_{\rm SL}$ in Eq. (69). The solid line shows the branching ratio where the $\mathcal{O}(\alpha_s^2 n_f)$ [or the $\mathcal{O}(\alpha_s^2\beta_0)$] improvements are included.

[2]Note, that n_f is replaced by $-3\beta_0/2$.

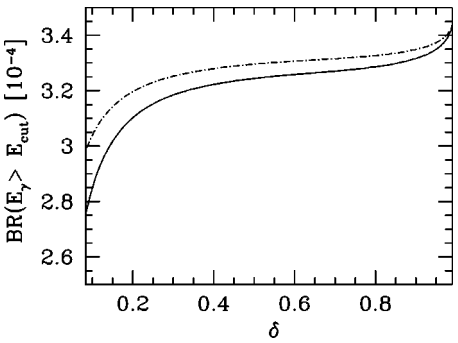

FIG. 8. Dependence of the branching ratio on the photon energy cut $E_{\rm cut}=(m_b/2)(1-\delta)$. The dash-dotted curve shows the NLL result, while the solid curve includes the $\mathcal{O}(\alpha_s^2 n_f)$ improvements. The renormalization scale is $\mu=4.8$ GeV.

One observes that for $\mu\approx 5.5$ GeV the $\mathcal{O}(\alpha_s^2 n_f)$ corrections vanish and that they are negative (positive) for smaller (larger) values of μ. In this context it is instructive to look at the decomposition of the result. For this reason we show in the left plot of Fig. 7 the $\mathcal{O}(\alpha_s^2 n_f)$ corrections where either $M_1^{(2)}$ and $M_2^{(2)}$ or $M_7^{(2)}$ is artificially set to zero which corresponds to the short-dashed and long-dashed curve, respectively. This illustrates that there is a large cancellation between the negative contribution from O_7 and the one from O_1 and O_2 which is, of course, also present in the amplitude D. The effect of the $\alpha_s^2 n_f$ corrections from the operator O_8 is significantly smaller and at most of the order of 2% in the considered interval for μ.

Figure 7 furthermore illustrates that the μ dependence of the $\mathcal{O}(\alpha_s^2 n_f)$ improved prediction for the branching ratio is somewhat flatter than in the NLL case if we restrict ourselves to $\mu\geqslant 4$ GeV. This is a welcome feature of our result, however, in general we cannot expect to reduce the μ dependence as the solid curve only represents a part of the $\mathcal{O}(\alpha_s^2)$ result. Indeed, we obtain a stronger μ dependence in the region below 4 GeV.

In Fig. 8 we show the dependence of the kinematical branching ratio on the photon energy cut. The dash-dotted line shows the NLL result, while the solid curve includes the order $\alpha_s^2 n_f$ improvements. We should mention at this point that we did not include any nonperturbative effects in the photon energy spectrum. The main purpose of this figure is to illustrate how the order $\alpha_s^2 n_f$ contributions modify the NLL result.

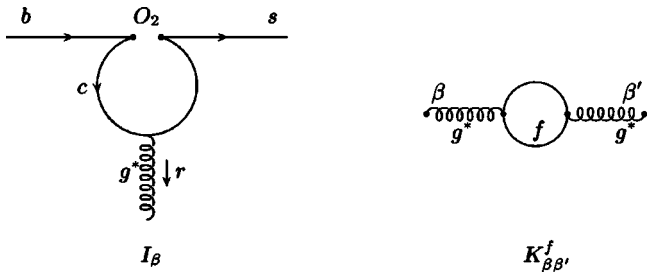

FIG. 9. The building blocks I_β and $K^f_{\beta\beta'}$ which are used in the calculation of the Feynman diagrams. The curly lines represent virtual gluons, whereas the letters b, c and s stand for the corresponding quark (f stands for a generic quark of mass m_f). Note that the external gluons are not amputated in the case of $K^f_{\beta\beta'}$.

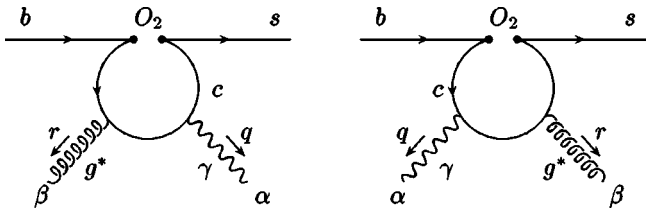

FIG. 10. The building block $J_{\alpha\beta}$ used in the calculation of the Feynman diagrams involving O_1 and O_2. The curly and wavy lines represent off-shell gluons and on-shell photons, respectively.

VI. CONCLUSIONS

In this paper a first step towards a complete NNLL calculation is undertaken and radiative corrections to the matrix elements of the operators O_1, O_2, O_7, and O_8 are computed. More precisely, we consider the contributions of order $\alpha_s^2 n_f$ which are induced by a massless quark loop. It is expected that these corrections, after replacing n_f by $-3\beta_0/2$, may give an important contribution to the full order α_s^2 corrections. Furthermore, motivated by the NLL analysis, we expect that the $\mathcal{O}(\alpha_s^2 n_f)$ corrections to the matrix elements numerically dominate the ones of the same order to the Wilson coefficient functions and to the anomalous dimension matrix.

In practice our calculation requires the evaluation of two- and three-loop diagrams in the case of O_7, O_8 and O_1, O_2, respectively. Furthermore, in order to obtain an infrared finite result in the case of O_7, also the contributions from the gluon bremsstrahlung and from the quark-pair emission process are taken into account which requires the evaluation of three- and four-particle phase space integrals, respectively. All calculations are performed analytically where an expansion in m_c/m_b is applied to the three-loop diagrams. For practical purposes this expansion is equivalent to the exact result.

As far as the numerical impact of our result is concerned, we observe a striking cancellation among the individual contributions at order $\alpha_s^2 n_f$. When using a photon energy cut of $E_{\rm cut}=m_b/20$, the $\mathcal{O}(\alpha_s^2 n_f)$ terms reduce (after replacing n_f by $-3\beta_0/2$) the branching ratio by -0.98% for $\mu=m_b=4.8$ GeV and lead to corrections of -3.9% and $+3.4\%$ for $\mu=3.0$ GeV and $\mu=9.6$ GeV, respectively.

ACKNOWLEDGMENTS

We would like to thank M. Misiak for making available to us his results for the renormalization constants of the operator mixing which provided important checks for our calculation. M.S. thanks T. Teubner for discussions on the quark-pair emission process. We thank A. Parkhomenko for carefully reading the manuscript. Our work was partially supported by the Swiss National Foundation and by RTN,

BBW-Contract No. 01.0357 and EC-Contract No. HPRN-CT-2002-00311 (EURIDICE).

APPENDIX A: BUILDING BLOCKS

The three-loop diagrams involving O_1 and O_2 as well as the two-loop graphs involving O_7 and O_8 can be calculated by using one or more of the building blocks I_β, $J_{\alpha\beta}$, and $K^f_{\beta\beta'}$ to be discussed in this appendix. The corresponding diagrams are shown in Figs. 9 and 10 where the color indices are suppressed.

The calculation of I_β is straightforward and yields

$$I_\beta = -\frac{g_s}{4\pi^2}\Gamma(\epsilon)\mu^{2\epsilon}e^{\gamma_E\epsilon}(1-\epsilon)e^{i\pi\epsilon}(r_\beta \not{r} - r^2\gamma_\beta)L\frac{\lambda}{2} \times \int_0^1 dx[x(1-x)]^{1-\epsilon}\left[r^2 - \frac{m_c^2}{x(1-x)} + i\delta\right]^{-\epsilon}, \quad \text{(A1)}$$

where r is the momentum of the virtual gluon emitted from the c-quark loop. In the three-loop diagrams shown in Fig. 1 (cf. Sec. II A), the free index β will be contracted with the corresponding index of the dressed gluon propagator $K^f_{\beta\beta'}$.

It is also quite simple to obtain the building block $K^f_{\beta\beta'}$ (i.e., the dressed gluon propagator) which can be cast into the form

$$K^f_{\beta\beta'} = -\frac{g_s^2}{2\pi^2}T\Gamma(\epsilon)e^{\gamma_E\epsilon}e^{i\pi\epsilon}\mu^{2\epsilon}\frac{1}{i}\frac{g_{\beta\beta'} - \dfrac{r_\beta r_{\beta'}}{r^2}}{r^2 + i\delta} \times \int_0^1 dx x(1-x)[x(1-x)r^2 - m_f^2 + i\delta]^{-\epsilon}, \quad \text{(A2)}$$

where m_f denotes the mass of the quarks and $T=\frac{1}{2}$. Note that this expression is independent of the gauge parameter ξ which enters the free gluon propagators in the construction of $K^f_{\beta\beta'}$, when working in an arbitrary R_ξ gauge.

The building block $J_{\alpha\beta}$ is somewhat more involved. Adopting the notation of Ref. [34], it reads (for an on-shell photon) [20]

$$J_{\alpha\beta} = \frac{eg_sQ_u}{16\pi^2}\Big[E(\alpha,\beta,r)\Delta i_5 + E(\alpha,\beta,q)\Delta i_6 - E(\beta,r,q)\frac{r_\alpha}{q\cdot r}\Delta i_{23} - E(\alpha,r,q)\frac{r_\beta}{q\cdot r}\Delta i_{25} - E(\alpha,r,q)\frac{q_\beta}{q\cdot r}\Delta i_{26}\Big]L\frac{\lambda}{2}, \quad \text{(A3)}$$

where q and r denote the momenta of the on-shell photon and the off-shell gluon, respectively. When inserted into the full diagrams in Fig. 2, the indices α and β will be contracted with the polarization vector ε of the photon and with the dressed gluon propagator $K^f_{\beta\beta'}$, respectively. The matrix $E(\alpha,\beta,r)$ is defined as

$$E(\alpha,\beta,r) = \frac{1}{2}(\gamma_\alpha\gamma_\beta \not{r} - \not{r}\gamma_\beta\gamma_\alpha), \quad \text{(A4)}$$

and the dimensionally regularized quantities Δi_k occurring in Eq. (A3) read

$$\begin{aligned}
\Delta i_5 &= 4B^+\int_S dxdy[4(q\cdot r)xy(1-x)\epsilon + r^2x(1-x)(1-2x)\epsilon + (1-3x)C]C^{-1-\epsilon},\\
\Delta i_6 &= 4B^+\int_S dxdy[-4(q\cdot r)xy(1-y)\epsilon - r^2x(2-2x+2xy-y)\epsilon - (1-3y)C]C^{-1-\epsilon},\\
\Delta i_{23} &= -\Delta i_{26} = 8B^+(q\cdot r)\int_S dxdyxy\epsilon C^{-1-\epsilon},\\
\Delta i_{25} &= -8B^+(q\cdot r)\int_S dxdyx(1-x)\epsilon C^{-1-\epsilon},
\end{aligned} \quad \text{(A5)}$$

where $B^+ = (1+\epsilon)\Gamma(\epsilon)e^{\gamma_E\epsilon}\mu^{2\epsilon}$ and C is given by

$$C = m_c^2 - 2xy(q\cdot r) - r^2x(1-x) - i\delta.$$

The integration over the Feynman parameters x and y is restricted to the simplex S, i.e., $y\in[0,1-x]$, $x\in[0,1]$. Because of the Ward identities, the quantities Δi_k are not independent of one another. Namely,

$$q^\alpha J_{\alpha\beta} = 0 \quad \text{and} \quad r^\beta J_{\alpha\beta} = 0$$

imply that Δi_5 and Δi_6 can be expressed as

$$\Delta i_5 = \Delta i_{23}, \quad \Delta i_6 = \frac{r^2}{q\cdot r}\Delta i_{25} + \Delta i_{26}. \quad \text{(A6)}$$

APPENDIX B: REGULARIZED THREE-LOOP RESULTS FOR $\langle s\gamma|O_2|b\rangle$

In Sec. II A we explained in some detail the calculation of the virtual three-loop corrections to $\langle s\gamma|O_2|b\rangle$. Here we give the results for the four gauge-invariant sets of graphs depicted in Figs. 1 and 2. The results read, using $z = m_c^2/m_b^2$ and $L = \ln(z)$,

$$M^{(2)}_{2,\mathrm{bare}}(1)=\left\{\frac{1}{\epsilon}\left[-\frac{1}{81\epsilon}-\frac{29}{243}+\frac{1}{6}(5+2L)z+\frac{1}{6}(5-2L+2L^2-2\pi^2)z^2+\frac{1}{81}(17+30L-18L^2+18\pi^2)z^3\right.\right.$$
$$\left.-\frac{i\pi}{27}(1-9z+9z^2-18Lz^2-10z^3+12Lz^3)\right]\left(\frac{m_b}{\mu}\right)^{-6\epsilon}+\left[-\frac{1063}{1458}+\frac{19\pi^2}{324}+\frac{1}{18}(61+4L-9L^2-10\pi^2)z\right.$$
$$+\frac{1}{18}[79-22L+28L^2-8L^3-9\pi^2-14L\pi^2-12\zeta(3)]z^2+\frac{1}{81}(63-27L-36L^2+24L^3-59\pi^2+42L\pi^2$$
$$\left.\left.+36\zeta(3))z^3-\frac{i\pi}{162}[58-441z-9(23+38L-6L^2-12\pi^2)z^2-12(4+3L+3L^2+6\pi^2)z^3]\right]+\mathcal{O}(z^4)\right\}$$
$$\times\left(\frac{\alpha_s}{\pi}\right)^2 C_F T n_f Q_d\langle s\gamma|O_7|b\rangle_{\mathrm{tree}}, \tag{B1}$$

$$M^{(2)}_{2,\mathrm{bare}}(2)=\left\{\frac{1}{\epsilon}\left[\frac{7}{162\epsilon}+\frac{5}{486}+\frac{1}{18}(3-\pi^2)z+\frac{2\pi^2}{9}z^{3/2}-\frac{1}{6}(6-6L+L^2)z^2+\frac{1}{324}(157-6L-144L^2-60\pi^2)z^3\right]\right.$$
$$\times\left(\frac{m_b}{\mu}\right)^{-6\epsilon}+\left[-\frac{1387}{1458}+\frac{11\pi^2}{72}+\frac{1}{54}[96-17\pi^2-126\zeta(3)]z+\frac{\pi^2}{27}[40-18L-72\ln(2)]z^{3/2}\right.$$
$$+\frac{1}{36}[213+102L-40L^2+8L^3+34\pi^2+96\zeta(3)]z^2-\frac{20\pi^2}{9}z^{5/2}+\frac{1}{324}[2799-995L-198L^2+192L^3$$
$$\left.\left.-10\pi^2-60L\pi^2-936\zeta(3)]z^3\right]+\mathcal{O}(z^{7/2})\right\}\left(\frac{\alpha_s}{\pi}\right)^2 C_F T n_f Q_d\langle s\gamma|O_7|b\rangle_{\mathrm{tree}}, \tag{B2}$$

$$M^{(2)}_{2,\mathrm{bare}}(3)=\left\{\frac{1}{\epsilon}\left[\frac{1}{36\epsilon}+\frac{137}{432}-\frac{1}{36}[18+24L+3L^2+2L^3-3\pi^2-6L\pi^2-24\zeta(3)]z-\frac{1}{36}[15+6L-6L^2+2L^3+6\pi^2\right.\right.$$
$$-6L\pi^2-24\zeta(3)]z^2+\frac{1}{36}(17-12L)z^3+\frac{i\pi}{36}(3-24z-6Lz-6L^2z+2\pi^2z-6z^2+12Lz^2-6L^2z^2+2\pi^2z^2$$
$$\left.-12z^3)\right]\left(\frac{m_b}{\mu}\right)^{-6\epsilon}+\left[\frac{6029}{2592}-\frac{17\pi^2}{144}-\frac{1}{1080}[7200+6240L-120L^2+220L^3-105L^4-2040\pi^2-1200L\pi^2\right.$$
$$+90L^2\pi^2+111\pi^4-4440\zeta(3)+1440L\zeta(3)]z-\frac{1}{2160}[15135-5790L-1050L^2+980L^3-210L^4-30\pi^2$$
$$-780L\pi^2+180L^2\pi^2+222\pi^4-4560\zeta(3)+2880L\zeta(3)]z^2+\frac{1}{72}(3-2L+72\pi^2)z^3$$
$$+\frac{i\pi}{432}\{411-4[786+192L+93L^2-24L^3-49\pi^2-12L\pi^2-72\zeta(3)]z+2[309+102L-186L^2+48L^3$$
$$\left.\left.-10\pi^2+24L\pi^2+144\zeta(3)]z^2+8(75-54L)z^3\}\right]+\mathcal{O}(z^4)\right\}\left(\frac{\alpha_s}{\pi}\right)^2 C_F T n_f Q_u\langle s\gamma|O_7|b\rangle_{\mathrm{tree}}, \tag{B3}$$

$$M^{(2)}_{2,\mathrm{bare}}(4)=\left\{\frac{1}{\epsilon}\left[\frac{1}{18\epsilon}+\frac{127}{432}-\frac{1}{36}[12+6L-L^3-\pi^2-3L\pi^2-12\zeta(3)]z-\frac{1}{36}[6-6L+3L^2-L^3+2\pi^2+24\zeta(3)]z^2\right.\right.$$
$$\left.-\frac{1}{324}(27+108L-81L^2-27\pi^2)z^3\right]\left(\frac{m_b}{\mu}\right)^{-6\epsilon}+\left[\frac{2839}{2592}+\frac{13\pi^2}{144}-\frac{1}{2160}[9480+2040L+180L^2-340L^3\right.$$
$$+105L^4+260\pi^2-720L\pi^2+30L^2\pi^2-439\pi^4-3360\zeta(3)-8640L\zeta(3)]z-\frac{8\pi^2}{3}z^{3/2}$$
$$+\frac{1}{4320}[29895-6270L-1410L^2+740L^3-210L^4+920\pi^2-480L\pi^2+120L^2\pi^2-52\pi^4-16320\zeta(3)$$

$$+4320L\zeta(3)]z^2+\frac{40\pi^2}{27}z^{5/2}-\frac{1}{216}[1358-477L-99L^2+90L^3+63\pi^2-18L\pi^2-432\zeta(3)]z^3\Big]+\mathcal{O}(z^{7/2})\Big\}$$

$$\times\left(\frac{\alpha_s}{\pi}\right)^2 C_F T n_f Q_u \langle s\gamma|O_7|b\rangle_{\text{tree}}. \tag{B4}$$

In these expressions, ζ denotes the Riemann ζ function with the value $\zeta(3)\approx 1.2020569$. $Q_u=2/3$ and $Q_d=-1/3$ are the electric charge factors of the up- and down-type quarks, respectively, while $C_F=4/3$ and $T=1/2$ are color factors.

APPENDIX C: CORRECTION FUNCTIONS NEEDED FOR THE NLL RESULT

The renormalization scale independent parts of the virtual corrections in NLL order precision, encoded in the functions $r_i^{(1)}$, appearing in Eq. (58), read

$$r_1^{(1)}=-\frac{1}{6}r_2^{(1)},$$

$$r_2^{(1)}=\frac{2}{243}\{-833+144\pi^2 z^{3/2}+[1728-180\pi^2-1296\zeta(3)+(1296-324\pi^2)L+108L^2+36L^3]z$$
$$+[648+72\pi^2+(432-216\pi^2)L+36L^3]z^2+[-54-84\pi^2+1092L-756L^2]z^3\}$$
$$+\frac{16\pi i}{81}\{-5+[45-3\pi^2+9L+9L^2]z+[-3\pi^2+9L^2]z^2+[28-12L]z^3\}+\mathcal{O}(z^{7/2}),$$

$$r_7^{(1)}=\frac{32}{9}-\frac{8}{9}\pi^2,$$

$$r_8^{(1)}=-\frac{4}{27}(-33+2\pi^2-6i\pi), \tag{C1}$$

where z is defined as $z=m_c^2/m_b^2$ and the symbol L denotes $L=\ln(z)$. The quantities $l_i^{(1)}$, appearing in Eq. (58), read

$$l_1^{(1)}=-\frac{1}{6}l_2^{(1)},\quad l_2^{(1)}=\frac{416}{81},\quad l_7^{(1)}=\frac{8}{3},\quad l_8^{(1)}=-\frac{32}{9}. \tag{C2}$$

Notice that $r_3^{(1)}$, $r_4^{(1)}$, $r_5^{(1)}$, and $r_6^{(1)}$, as well as $l_3^{(1)}$, $l_4^{(1)}$, $l_5^{(1)}$, and $l_6^{(1)}$ are not needed in the approximation $C_i^{\text{eff}}(\mu)=0$ ($i=3,4,5,6$).

The functions f_{ij} needed for Eq. (65) are taken from Ref. [12] and are listed here for completeness. Note that $f_{77}(\delta)$ differs from the one given in Ref. [12] in order to be compatible with our r_7 given in Eq. (C1).[3]

$$f_{11}(\delta)=\frac{1}{36}f_{22}(\delta),\quad f_{12}(\delta)=-\frac{1}{3}f_{22}(\delta),\quad f_{17}(\delta)=-\frac{1}{6}f_{27}(\delta),\quad f_{18}(\delta)=-\frac{1}{6}f_{28}(\delta),$$

$$f_{22}(\delta)=\frac{16z}{27}\left[\delta\int_0^{(1-\delta)/z}dt(1-zt)\left|\frac{G(t)}{t}+\frac{1}{2}\right|^2+\int_{(1-\delta)/z}^{1/z}dt(1-zt)^2\left|\frac{G(t)}{t}+\frac{1}{2}\right|^2\right],$$

$$f_{27}(\delta)=-\frac{8z^2}{9}\left[\delta\int_0^{(1-\delta)/z}dt\,\mathrm{Re}\left(G(t)+\frac{t}{2}\right)+\int_{(1-\delta)/z}^{1/z}dt(1-zt)\mathrm{Re}\left(G(t)+\frac{t}{2}\right)\right],$$

$$f_{28}(\delta)=-\frac{1}{3}f_{27}(\delta),$$

[3]The additional, δ-independent addend appearing in our $f_{77}(\delta)$ is such that $f_{77}(1)$ vanishes: the contribution of $f_{77}(\delta)$ at $\delta=1$ is already absorbed into our r_7.

$$f_{77}(\delta)=\frac{10}{3}\delta+\frac{1}{3}\delta^2-\frac{2}{9}\delta^3+\frac{1}{3}\delta(\delta-4)\ln(\delta)-\frac{31}{9},$$

$$f_{78}(\delta)=\frac{8}{9}\left[\mathrm{Li}_2(1-\delta)-\frac{\pi^2}{6}-\delta\ln(\delta)+\frac{9}{4}\delta-\frac{1}{4}\delta^2+\frac{1}{12}\delta^3\right],$$

$$f_{88}(\delta)=\frac{1}{27}\left\{-2\ln\left(\frac{m_b}{m_s}\right)[\delta^2+2\delta+4\ln(1-\delta)]+4\,\mathrm{Li}_2(1-\delta)-\frac{2\pi^2}{3}-\delta(2+\delta)\ln(\delta)+8\ln(1-\delta)+7\delta+3\delta^2-\frac{2}{3}\delta^3\right\}, \tag{C3}$$

where the function $G(t)$ is defined through

$$G(t)=\begin{cases}-2\arctan^2\left(\sqrt{\dfrac{t}{4-t}}\right) & \text{for } t<4,\\ -\dfrac{\pi^2}{2}+2\ln^2\left[\dfrac{1}{2}(\sqrt{t}+\sqrt{t-4})\right]-2i\pi\ln\left[\dfrac{1}{2}(\sqrt{t}+\sqrt{t-4})\right] & \text{for } t\geqslant 4.\end{cases} \tag{C4}$$

The functions f_{ij} associated with the operators O_3-O_6 are not needed in our approximation. Note that in the numerics we set m_s equal to zero in all terms except $f_{88}(\delta)$, where a value of $m_b/m_s=50$ is chosen.

APPENDIX D: $\mathcal{O}(\alpha_s^2 n_f)$ CONTRIBUTIONS TO VARIOUS Z FACTORS

In this appendix we give the results for the $\mathcal{O}(\alpha_s^2 n_f)$ contributions for various Z factors entering the calculation of the counterterm $M_{7,\mathrm{ct}_2}^{(2),(a)}$ in Eq. (45) in Sec. III. For the meaning of the various terms, see the text after Eq. (45). The $\mathcal{O}(\alpha_s^2 n_f)$ contributions to the relevant Z factors read

$$\delta Z_{2,b}^{(2),n_f}=\left(\frac{\alpha_s}{\pi}\right)^2\frac{C_F T n_f}{288}\left\{\frac{18}{\epsilon}\left[1-4\ln(f)-8\ln\left(\frac{m_b}{\mu}\right)\right]+443+30\pi^2+96\ln(f)+72\ln^2(f)-264\ln\left(\frac{m_b}{\mu}\right)+288\ln(f)\ln\left(\frac{m_b}{\mu}\right)\right.$$
$$\left.+432\ln^2\left(\frac{m_b}{\mu}\right)\right\}, \tag{D1}$$

$$\delta Z_{2,s}^{(2),n_f}=\left(\frac{\alpha_s}{\pi}\right)^2\frac{C_F T n_f}{96}\left\{\frac{6}{\epsilon}\left[1-4\ln(f)-8\ln\left(\frac{m_b}{\mu}\right)\right]-5+2\pi^2-44\ln(f)+12\ln^2(f)+24\ln(f)\ln(r)-88\ln\left(\frac{m_b}{\mu}\right)\right.$$
$$\left.+96\ln(f)\ln\left(\frac{m_b}{\mu}\right)+48\ln(r)\ln\left(\frac{m_b}{\mu}\right)+144\ln^2\left(\frac{m_b}{\mu}\right)\right\}, \tag{D2}$$

$$\delta Z_{m_b}^{\mathrm{on},(2),n_f}=\left(\frac{\alpha_s}{\pi}\right)^2\frac{C_F T n_f}{96}\left[71+8\pi^2-104\ln\left(\frac{m_b}{\mu}\right)+48\ln^2\left(\frac{m_b}{\mu}\right)+\frac{10}{\epsilon}-\frac{12}{\epsilon^2}\right], \tag{D3}$$

$$\delta Z_{77}^{(2),n_f}=\left(\frac{\alpha_s}{\pi}\right)^2\frac{C_F n_f T}{36\epsilon}\left(\frac{6}{\epsilon}-7\right), \tag{D4}$$

with $r=m_s^2/m_b^2$ and $f=m_f^2/m_b^2$.

APPENDIX E: IMPLEMENTING THE PHOTON ENERGY CUT-OFF IN THE $\mathcal{O}(\alpha_s^2 n_f)$ TERMS

In this appendix we provide the formulas which are needed to calculate the $\mathcal{O}(\alpha_s^2 n_f)$ piece of the kinematical branching ratio $\mathrm{BR}(b\to X_s\gamma)_{E_\gamma\geqslant E_{\mathrm{cut}}}$, where E_{cut} represents a cutoff on the photon energy. As can be seen from the structure of Eq. (67), this amounts to calculate $\Gamma_{77}^{(2),n_f}(b\to X_s\gamma)_{E_\gamma\leqslant E_{\mathrm{cut}}}$, which is contained in the quantity D of Eq. (67).

Note that only the gluon bremsstrahlung- and the quark-pair emission processes enter the calculation for $\Gamma_{77}^{(2),n_f}(b\to X_s\gamma)_{E_\gamma\leqslant E_{\mathrm{cut}}}$ as the photon energy in the virtual contributions is concentrated at $m_b/2$. The $\mathcal{O}(\alpha_s^2 n_f)$ contribution to $\Gamma_{77}^{(2),n_f}(b\to X_s\gamma)_{E_\gamma\leqslant E_{\mathrm{cut}}}$ can be written in the form

$$\Gamma_{77}^{(2),n_f}(b\to X_s\gamma)_{E_\gamma\leqslant E_{\rm cut}}=\Gamma_{77}^0[\hat\Gamma_{77}^{(2),(b)}(E_\gamma\leqslant E_{\rm cut}) + \hat\Gamma_{77}^{(2),(c)}(E_\gamma\leqslant E_{\rm cut})], \quad \text{(E1)}$$

where (b) and (c) denote the gluon bremsstrahlung- and the quark-pair emission process, respectively, and Γ_{77}^0 is given in Eq. (32). As in Sec. III we use a regulator mass m_f for the secondary quark-antiquark pair which means that Eq. (E1) can be calculated in $d=4$ dimensions and with $m_s=0$.

The calculation for the gluon bremsstrahlung piece $\hat\Gamma_{77}^{(2),(b)}(E_\gamma\leqslant E_{\rm cut})$ is straightforward. Adopting the notation

$$E_{\rm cut}=\frac{m_b}{2}(1-\delta)=E_{\rm max}(1-\delta), \quad \text{(E2)}$$

the result reads

$$\hat\Gamma_{77}^{(2),(b)}(E_\gamma\leqslant E_{\rm cut})=\left(\frac{\alpha_s}{4\pi}\right)^2\frac{4C_FTn_f}{9}[31-30\delta-3\delta^2+2\delta^3 + 21\ln(\delta)+12\delta\ln(\delta)-3\delta^2\ln(\delta)+6\ln^2(\delta)] \times\left[\ln(f)+2\ln\left(\frac{m_b}{\mu}\right)\right], \quad \text{(E3)}$$

with $f=m_f^2/m_b^2$.

The calculation for $\hat\Gamma_{77}^{(2),(c)}(E_\gamma\leqslant E_{\rm cut})$ is somewhat more involved but still can be performed analytically, yielding

$$\begin{aligned}\hat\Gamma_{77}^{(2),(c)}(E_\gamma\leqslant E_{\rm cut})=&\left(\frac{\alpha_s}{4\pi}\right)^2\frac{2C_FTn_f}{9}\{-147-9\pi^2+48\zeta(3)\\ &-48\,{\rm Li}_3(\delta)+54\,{\rm Li}_2(\delta)-\ln(\delta)[85-4\pi^2\\ &-54\ln(1-\delta)-24\,{\rm Li}_2(\delta)]+13\ln^2(\delta)\\ &+12\ln^3(\delta)+\delta[160+4\pi^2-24\,{\rm Li}_2(\delta)\\ &-24\ln(1-\delta)\ln(\delta)-94\ln(\delta)+36\ln^2(\delta)]\\ &+\delta^2[1-\pi^2+6\,{\rm Li}_2(\delta)+6\ln(1-\delta)\ln(\delta)\\ &+19\ln(\delta)-9\ln^2(\delta)]-\delta^3[14-4\ln(\delta)]\\ &-2\ln(f)[31-30\delta-3\delta^2+2\delta^3+21\ln(\delta)\\ &+12\delta\ln(\delta)-3\delta^2\ln(\delta)+6\ln^2(\delta)]\}. \quad \text{(E4)}\end{aligned}$$

Note that the sum of $\hat\Gamma_{77}^{(2),(b)}(E_\gamma\leqslant E_{\rm cut})$ and $\hat\Gamma_{77}^{(2),(c)}(E_\gamma\leqslant E_{\rm cut})$ is finite in the limit $m_f\to 0$. This completes the calculation of $\Gamma_{77}^{(2),n_f}(b\to X_s\gamma)_{E_\gamma\leqslant E_{\rm cut}}$, defined in Eq. (E1).

We note that differentiating $\Gamma_{77}^{(2),n_f}(b\to X_s\gamma)_{E_\gamma\leqslant E_{\rm cut}}$ with respect to the photon energy cut $E_{\rm cut}$ generates the corresponding term of order $\alpha_s^2 n_f$ to the photon energy spectrum. The result we obtain is in complete agreement with Eq. (9) of Ref. [25], where $\mathcal{O}(\alpha_s^2 n_f)$ corrections to the photon energy spectrum were calculated.

[1] CLEO Collaboration, S. Chen *et al.*, Phys. Rev. Lett. **87**, 251807 (2001).
[2] Belle Collaboration, K. Abe *et al.*, Phys. Lett. B **511**, 151 (2001).
[3] ALEPH Collaboration, R. Barate *et al.*, Phys. Lett. B **429**, 169 (1998).
[4] BABAR Collaboration, B. Aubert *et al.*, hep-ex/0207074.
[5] BABAR Collaboration, B. Aubert *et al.*, hep-ex/0207076.
[6] C. Jessop, SLAC-PUB-9610.
[7] A. Czarnecki and W.J. Marciano, Phys. Rev. Lett. **81**, 277 (1998).
[8] A.L. Kagan and M. Neubert, Eur. Phys. J. C **7**, 5 (1999).
[9] K. Baranowski and M. Misiak, Phys. Lett. B **483**, 410 (2000).
[10] P. Gambino and U. Haisch, J. High Energy Phys. **09**, 001 (2000); **10**, 020 (2001).
[11] T. Hurth, hep-ph/0212304.
[12] K.G. Chetyrkin, M. Misiak, and M. Münz, Phys. Lett. B **400**, 206 (1997); **425**, 414(E) (1998).
[13] M. Ciuchini, G. Degrassi, P. Gambino, and G.F. Giudice, Nucl. Phys. **B527**, 21 (1998).
[14] F.M. Borzumati and C. Greub, Phys. Rev. D **58**, 074004 (1998); **59**, 057501 (1998).
[15] A.J. Buras, A. Kwiatkowski, and N. Pott, Nucl. Phys. **B517**, 353 (1998); Phys. Lett. B **414**, 157 (1997); **434**, 459(E) (1998).
[16] P. Gambino and M. Misiak, Nucl. Phys. **B611**, 338 (2001).
[17] A.J. Buras, A. Czarnecki, M. Misiak, and J. Urban, Nucl. Phys. **B631**, 219 (2002).
[18] A. Ali, E. Lunghi, C. Greub, and G. Hiller, Phys. Rev. D **66**, 034002 (2002).
[19] A.J. Buras, M. Misiak, M. Münz, and S. Pokorski, Nucl. Phys. **B424**, 374 (1994).
[20] C. Greub, T. Hurth, and D. Wyler, Phys. Rev. D **54**, 3350 (1996).
[21] M. Beneke and V.M. Braun, Phys. Lett. B **348**, 513 (1995).
[22] S.J. Brodsky, G.P. Lepage, and P.B. Mackenzie, Phys. Rev. D **28**, 228 (1983).
[23] M.E. Luke, M.J. Savage, and M.B. Wise, Phys. Lett. B **345**, 301 (1995).
[24] A. Czarnecki and K. Melnikov, Phys. Rev. D **59**, 014036 (1999).
[25] Z. Ligeti, M.E. Luke, A.V. Manohar, and M.B. Wise, Phys. Rev. D **60**, 034019 (1999).
[26] C. Greub and P. Liniger, Phys. Lett. B **494**, 237 (2000).
[27] H.H. Asatryan, H.M. Asatrian, C. Greub, and M. Walker, Phys. Rev. D **65**, 074004 (2002).
[28] M. Misiak (private communication).
[29] A. Falk, M. Luke, and M. Savage, Phys. Rev. D **49**, 3367 (1994); I.I. Bigi, M. Shifman, N.G. Uraltsev, and A.I. Vainshtein, Phys. Rev. Lett. **71**, 496 (1993); A.V. Manohar and M.B. Wise, Phys. Rev. D **49**, 1310 (1994); A. Falk, M. Luke, and M. Savage, *ibid.* **53**, 2491 (1996).
[30] M.B. Voloshin, Phys. Lett. B **397**, 275 (1997); Z. Ligeti, L. Randall, and M.B. Wise, *ibid.* **402**, 178 (1997); A.K. Grant,

A.G. Morgan, S. Nussinov, and R.D. Peccei, Phys. Rev. D **56**, 3151 (1997); G. Buchalla, G. Isidori, and S.J. Rey, Nucl. Phys. **B511**, 594 (1998).
[31] A. Ali and C. Greub, Z. Phys. C **49**, 431 (1991); Phys. Lett. B **259**, 182 (1991); **361**, 146 (1995).
[32] N. Pott, Phys. Rev. D **54**, 938 (1996).
[33] Y. Nir, Phys. Lett. B **221**, 184 (1989).
[34] H. Simma and D. Wyler, Nucl. Phys. **B344**, 283 (1990).